



A new blind source separation framework for signal analysis and artifact rejection in functional Near-Infrared Spectroscopy

Alexander von Lühmann^{a,b,*}, Zois Boukouvalas^{c,d}, Klaus-Robert Müller^{a,f,g,**}, Tülay Adalı^{e,***}

^a Machine Learning Dept., Berlin Institute of Technology, Berlin, Germany

^b Neurophotonics Center, Biomedical Engineering, Boston University, Boston, MA, 02215, USA

^c Dept. of ENME, University of Maryland, College Park, MD, 20742, USA

^d Dept. of Mathematics and Statistics, American University, Washington, DC, 20016, USA

^e Dept. of CSEE, University of Maryland, Baltimore County, Baltimore, MD, 21250, USA

^f Dept. of Brain and Cognitive Engineering, Korea University, Seoul, 02841, South Korea

^g Max Planck Institute for Informatics, Saarbrücken, 66123, Germany

ARTICLE INFO

Keywords:

fNIRS
Neuroimaging in motion
Blind source separation
Entropy rate bound minimization
Multimodality
Machine learning
Artifact removal

ABSTRACT

In the analysis of functional Near-Infrared Spectroscopy (fNIRS) signals from real-world scenarios, artifact rejection is essential. However, currently there exists no gold-standard. Although a plenitude of methodological approaches implicitly assume the presence of latent processes in the signals, elaborate Blind-Source-Separation methods have rarely been applied. A reason are challenging characteristics such as Non-instantaneous and non-constant coupling, correlated noise and statistical dependencies between signal components. We present a novel suitable BSS framework that tackles these issues by incorporating A) Independent Component Analysis methods that exploit both higher order statistics and sample dependency, B) multimodality, i.e., fNIRS with accelerometer signals, and C) Canonical-Correlation Analysis with temporal embedding. This enables analysis of signal components and rejection of motion-induced physiological hemodynamic artifacts that would otherwise be hard to identify. We implement a method for Blind Source Separation and Accelerometer based Artifact Rejection and Detection (BLISSA²RD). It allows the analysis of a novel n-back based cognitive workload paradigm in freely moving subjects, that is also presented in this manuscript. We evaluate on the corresponding data set and simulated ground truth data, making use of metrics based on 1st and 2nd order statistics and SNR and compare with three established methods: PCA, Spline and Wavelet-based artifact removal. Across 17 subjects, the method is shown to reduce movement induced artifacts by up to two orders of magnitude, improves the SNR of continuous hemodynamic signals in single channels by up to 10 dB, and significantly outperforms conventional methods in the extraction of simulated Hemodynamic Response Functions from strongly contaminated data. The framework and methods presented can serve as an introduction to a new type of multivariate methods for the analysis of fNIRS signals and as a blueprint for artifact rejection in complex environments beyond the applied paradigm.

1. Introduction

Functional Near-Infrared Spectroscopy (fNIRS) or -imaging (fNIRI) is an optical neuroimaging technology that enables non-invasive local measurements of hemodynamic changes, i.e., oxy- (HbO) and deoxy-hemoglobin (HbR), in cortical brain areas. Within the last decades, fNIRS has been established as a research tool in medicine and neuroscience (Boas et al., 2001; Ferrari et al., 2004; Wolf et al., 2007; Hamaoka et al.,

2007; Hoshi, 2007; Scholkmann et al., 2014a) and now enables long-term non-invasive functional brain imaging at a good temporal resolution and relatively low cost without any known hazard or risks. New fNIRS device generations are becoming more miniaturized and wearable, also providing additional modalities like accelerometer or bioelectric signals (Muehlemann et al., 2008; Safaie et al., 2013; von Lühmann et al., 2015; von Lühmann et al., 2017; Wyser et al., 2017), and expand the spectrum of fNIRS beyond static and toward ambulatory

* Corresponding author. Machine Learning Dept., Berlin Institute of Technology, Berlin, Germany.

** Corresponding author. Machine Learning Dept., Berlin Institute of Technology, Berlin, Germany.

*** Corresponding author. Dept. of CSEE, University of Maryland, Baltimore County, Baltimore, USA.

E-mail addresses: avonluh@gmail.com (A. von Lühmann), klaus.r.mueller@googlemail.com (K.-R. Müller), adali@umbc.edu (T. Adalı).

domains. Important implications result for both medical/clinical and scientific fields, for instance in the study of brain function and disorders (Boushel et al., 2001; Irani et al., 2007), emerging pervasive healthcare and telemedicine (Zheng et al., 2014; Andreu-Perez et al., 2015), neuroergonomics (Parasuraman, 2003) and (hybrid) brain-computer interfaces (Pfurtscheller et al., 2010; Fazli et al., 2012; Müller-Putz et al., 2015).

The recovery of evoked brain activity from measured fNIRS signals is crucial, as neural task-related responses are masked by various physiological and non-physiological components which are often of equal or higher magnitude (see (Scholkmann et al., 2014a; Tachtsidis and Scholkmann, 2016) and Fig. 1). In fNIRS applications with moving

subjects, this gains further importance, as changing environmental and behavioral conditions add significant non-stationarities (von Bünaü et al., 2009). As the majority of studies until today has been conducted with fiber-optical instruments in sitting subjects, many methods in fNIRS literature provide a remedy only for one major subclass of movement artifacts: Optical decoupling between optodes and scalp that leads to instantaneous virtual variations of chromophore concentrations in the form of fast transient changes and sudden baseline shifts. We denote these as *Direct Movement Artifacts* (DMA), see also Fig. 1. With the rise of new lightweight wearable equipment and ambulatory applications, a second class of artifacts becomes increasingly important, but has only been tackled exceptionally so far: Motion-induced slow,

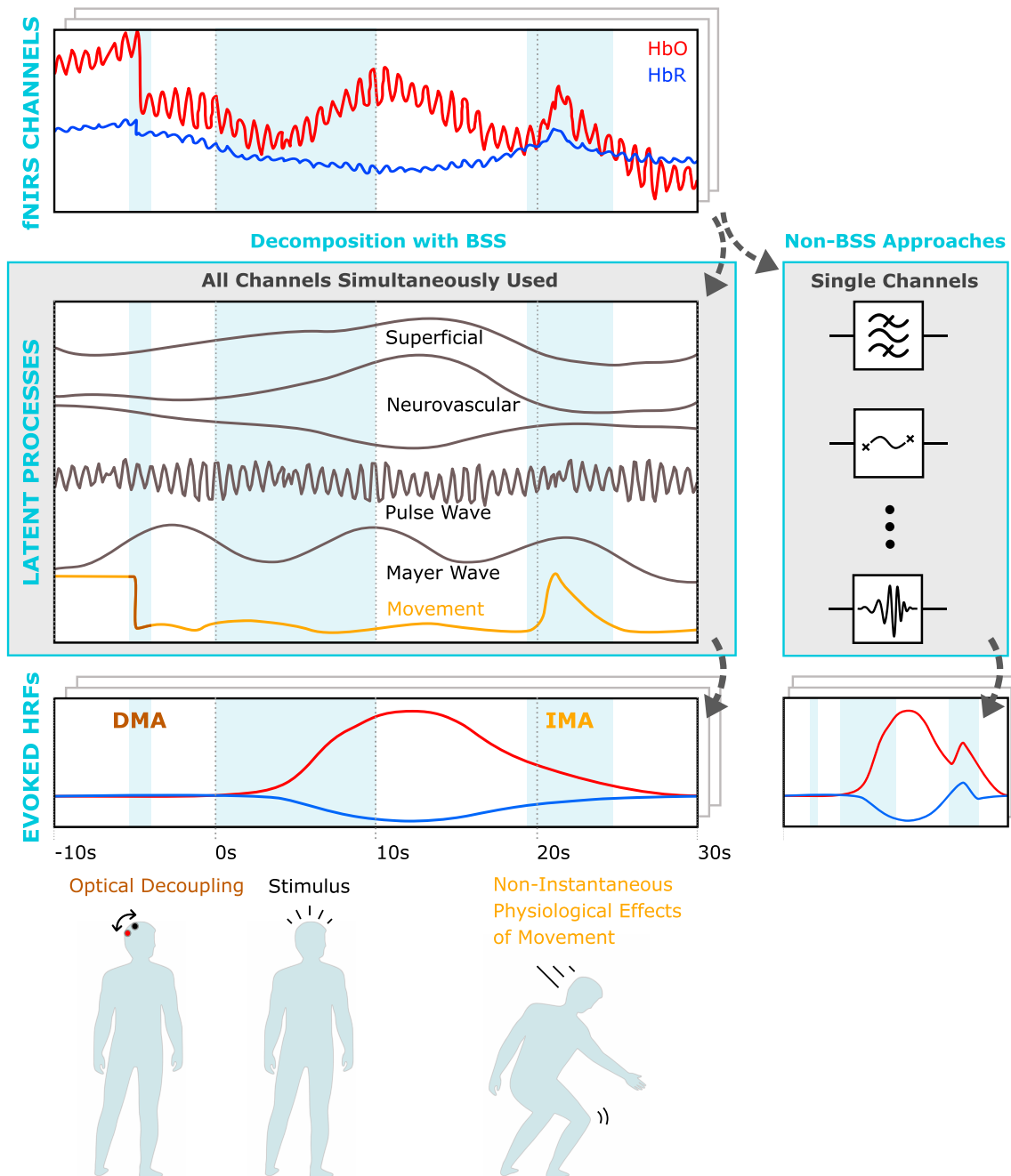


Fig. 1. Left: Schematic exemplary decomposition of fNIRS signals into components using all available channels in a data-driven BSS analysis. As a novel stand-alone approach or as a supplementary preprocessing alternative to non-BSS approaches that aim to denoise data in HRF-regression based GLM analysis. Illustration of the modulation of distinct components due to different types of movement artifacts: (DMA) direct, due to optode shifts and decoupling, (IMA) indirect, due to non-instantaneous motion induced physiological effects (focus of this work). Right: Conventional approaches, which often manipulate signals individually in the channel-domain, typically targeting only DMA.

non-instantaneous physiological processes (see also Fig. 1, IMA) that modulate partial blood pressure, scalp and cerebral blood flow/blood volume (CBF/CBV). We denote these as *indirect movement artifacts* (IMA). Once data contamination is detected, trials are often entirely rejected (Samek et al., 2017). However, when there are few trials or many movements, this is not an option.

There is currently no gold standard for the extraction of continuous evoked hemodynamic brain signals or Hemodynamic Response Functions (HRF) from masking noise components and movement artifacts. Univariate approaches include moving standard deviation and spline interpolation (Scholkmann et al., 2010), wavelet filtering (Molavi and Dumont, 2012), Kalman filtering (Izzetoglu et al., 2010), and correlation-based approaches (Cui et al., 2010). A promising class of multivariate methods makes use of complementary signals; either by performing regression or adaptive filtering with accelerometer signals (Virtanen et al., 2011; Metz et al., 2015) or in multi-distance (MD) approaches using multiple source-detector separations (Saager and Berger, 2005; Zhang et al., 2009; Scholkmann et al., 2014b) for the rejection of superficial components, e.g., those originating from the scalp. Scholkmann et al., 2014 gave a broad overview of univariate and multivariate methods for correction in fNIRS (Scholkmann et al., 2014a) and Brigadoi et al., 2014 compared multiple univariate motion correction techniques (Brigadoi et al., 2014). The majority of approaches implicitly assume the presence of latent physiological or non-physiological artefactual components, but manipulate signals in the channel domain. In contrast to other neuroimaging fields, elaborate Blind-Source Separation (BSS)-based methods are yet comparatively underrepresented in fNIRS, although they explicitly aim to identify latent processes. While Principal Component Analysis (PCA)-based approaches have successfully been applied to reduce superficial contributions from blood flow in static scenarios (Zhang et al., 2005; Franceschini et al., 2006), more complex methods such as Independent Component Analysis (ICA) have mainly served as an alternative to averaging for the extraction of typical fast or slow evoked responses from a high number of time-locked epochs (Morren et al., 2004; Medvedev et al., 2008; Akgül et al., 2006) or channels (e.g., 212 channels in a DOT system (Markham et al., 2009), 650 wavelengths in a broadband fNIRS (Schelkanova and Toronov, 2012)). When applied to remove extracerebral signals (Kohno et al., 2007), Virtanen concluded that (Fast)ICA typically performs worse than or equal to PCA (Virtanen et al., 2009).

Weak ICA performance is due to a variety of fNIRS signal characteristics that pose serious challenges to many standard BSS approaches, depending on their limitations and the assumptions and statistics in the underlying model (see also simulations in 5.3). Among the challenges in the signals are non-instantaneous and non-constant coupling, correlated noise (Huppert, 2016) and source dependencies. For a successful decomposition, it is crucial to select ICA algorithms that take the right type of diversities into account. As a consequence, to the best of our knowledge, there exists no elaborate BSS framework for the data-driven analysis and decomposition of single-trial fNIRS data so far. Ideally, such a framework enables extraction and analysis of functionally distinct components without affecting others — even when they share the same frequency band. Such a framework could be a useful tool for preprocessing/de-noising as well as for the general analysis of fNIRS signals components: either in combination with or complementary to conventional General Linear Model (GLM)-based HRF regression. Also, by taking advantage of complementary multimodal signals, it could facilitate the identification of artefactual processes that are otherwise hard to separate from the evoked hemodynamic responses, such as many indirect movement artifacts. We present an approach toward such a framework by combining

- Independent Component Analysis (ICA) methods that exploit both higher order statistics (HOS) and sample dependency by using mutual information rate as a unifying framework for source decomposition (Adali et al., 2014, 2015; Fu et al., 2014a),

- multimodality — here complementing fNIRS with accelerometer signals — assuming the presence of pairs of shared processes, and
- Canonical-Correlation Analysis (CCA) with temporal embedding to robustly extract the corresponding components.

As *fNIRS in motion* is a domain just emerging, there are currently no suitable datasets available that provide both evoked neuronal hemodynamic responses and well-controlled movement conditions, and certainly not multimodal data. For the purpose, we present a novel, custom-tailored experimental cognitive workload paradigm with freely moving subjects and use this unique data set for quantitative and qualitative evaluation of the proposed framework.

Purpose of this manuscript is to provide a general BSS framework for the data-driven analysis of fNIRS signals that can be used both supplementary to and independently from conventional approaches. We apply this Blind Source Separation framework to Accelerometer based Artifact Rejection and Detection (BLISSA²RD), tackling the challenge of indirect movement artifacts and pointing out challenging signal characteristics and possible solutions on the way.

The manuscript is structured as follows: In the methods section, we identify and discuss fNIRS signal components and challenging signal characteristics (subsections 2.1/2.2) and introduce the employed mathematical models (subsection 2.3). In 2.4 we propose the BSS-framework for fNIRS and its application in BLISSA²RD, tackling indirect movement artifacts. The new experimental paradigm and data set used for evaluation are presented in 2.5, followed by the applied evaluation metrics in 2.6. Section 3 then covers qualitative and quantitative evaluation results, followed by a discussion and conclusion.

2. Methods

2.1. fNIRS signal components

When performing BSS to extract underlying processes from fNIRS signals, a classification of expected components can help with interpretation in the source domain (see Fig. 2). For those of physiological origin, we adopt a classification scheme from Scholkmann et al. (2014a) and differentiate between six non-stationary physiological components C1 – C6 by categorizing them into classes as

1. *Source* (intracerebral vs. extracerebral),
2. *Stimulus/task relation* (evoked vs. non-evoked) and
3. *Cause* (neuronal vs. Systemic).

From the perspective of artifact rejection, it makes sense to extend this classification to components of non-physiological origin NC1 – NC3, typically introduced in the acquisition processes: *environmental influences*, *instrumentation noise* (usually stationary) and *changes in acquisition geometry* (e.g., optical decoupling, conventional movement artifacts).

Both types of components C_x and NC_x originate from different domains, i.e., that of physiological chromophore concentrations and that of raw signal intensities, respectively. Both are non-linearly linked to each other by the modified Beer-Lambert Law (mBLL) (Delpy et al., 1988). Variations in NC_x lead to virtual changes in the chromophore concentration domain. Commonly, careful instrumentation design robustifies against NC1 – NC2. Low- or band-pass filtering of fNIRS signals with a typical cut-off frequency around 0.2 Hz is common practice to minimize non-evoked components C4 – C6. Then, univariate and multivariate methods (Brigadoi et al., 2014; Scholkmann et al., 2014a) are used to mitigate systemic cerebral & extracerebral components (C2, C3, C5, C6) and direct movement artifacts due to optode shifts (NC3).

2.2. Challenging fNIRS signal characteristics

For (multimodal) BSS analysis, several challenging properties of fNIRS signals have to be taken into account, some of which can be

exemplified in the observation of combined raw fNIRS intensity and accelerometer signals (see Fig. 3):

- Single channels include both spatially specific and global unspecific components of neuronal or systemic, cerebral or extracerebral origin (C1-6). These are subject to
- Non-instantaneous, non-constant and non-linear coupling of the underlying physiological processes. Global and local systemic signals are non-simultaneously mixed into channels with spatially and behaviorally dependent delays and morphology as they non-instantaneously disperse along the arteriole system and depend i.e. on relative orientation and movement speed of the head and body (e.g., the pulse wave or blood-pooling effects).
- Correlated (pink) noise and sample dependency due to strong systemic periodic physiological components in the fNIRS signal (C5 and C6, e.g., the heart beat) (Huppert, 2016) collide with the assumption of Gaussian (white) noise and independent samples in the majority of applied models.
- Under-determined problem: Ideally, BSS approaches require an equal or higher number of measured signals than latent factors. As in EEG, it is often questionable whether this condition is fulfilled.
- Dependency between fNIRS sources: The assumption of independence in ICA collides with the fact that several underlying physiological processes in the fNIRS signals are not entirely separable and independent but form an interacting network of interlinked statistically dependent processes (Huppert, 2016; Scholkmann et al., 2014a).

Due to these properties, even the most elaborate BSS approaches might not achieve an ideal decomposition. From a Signal to Noise Ratio (SNR) perspective this is, however, not required: Source separation into subsets of the same or similar categories can already enable reliable artifact rejection and thus increase the overall SNR. This is the approach of BLISSA²RD, which identifies and then rejects subsets of movement-induced changes within the fNIRS signals, including but not limited to those due to blood-pooling.

2.3. Mathematical models

The Generative Linear Model. A commonly used abstract mathematical model for the generation of macroscopic neuroimaging data such as EEG, MEG, fMRI, and fNIRS represents the measured data as a linear mixture of functionally distinct processes (Parra et al., 2005). These generative or forward models factorize observed measurement data into latent factors (components) with a temporal signature and their corresponding spatial activation patterns. Please be aware of the difference between the following purely data-driven generative approach and the conventional supervised General Linear Model (GLM) for HRF regression in fNIRS (Josephs et al., 1997; Calhoun et al., 2001; Ye et al., 2009). While the latter includes a-priori information such as experimental

stimulus time structure and (canonical) shapes of the HRF, we work solely with the statistics of the data in a completely unsupervised manner. In the following, we therefore use the term “generative linear model” in the context of Machine Learning driven linear mixing models, and “General Linear Model (GLM)” when referring to the commonly employed regression model that is specific to the fNIRS/fMRI domain.

We will denote observed raw fNIRS data samples of time point t and channel n with scalars $x_n(t)$ and accelerometer samples respectively with $z_n(t)$. As the notation is congruent for both signals x and z , we will continue it exemplary for x only. We denote the observation matrix with data from all time points T_x and recorded channels N_x as $X \in \mathbb{R}^{N_x \times T_x}$, its row vectors as $x_n \in \mathbb{R}^{T_x}$ and its column vectors as $x(t) \in \mathbb{R}^{N_x}$. In raw fNIRS intensity signals, $N_x = C_x \cdot \Lambda_x$ consists of the number of optode pairs C_x and the number of recorded wavelengths Λ_x . Usually, the two modalities differ both in the number of channels and sampling rate $N_x \neq N_z$ and $T_x \neq T_z$. We assume the presence of $K_x \geq 1$ latent factors and denote these by $s_n \in \mathbb{R}^{K_x}$ and in analogy to above for all time points and factors by $S_x \in \mathbb{R}^{K_x \times T_x}$. Then, the noiseless linear forward model in a matrix notation can be expressed by

$$X = A_x S_x \tag{1}$$

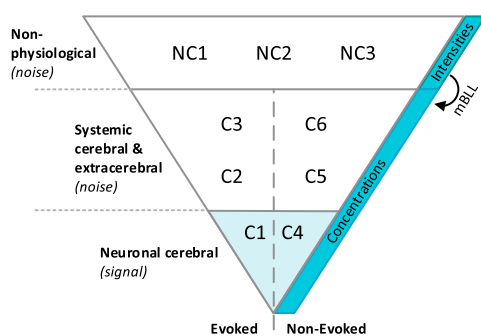
and the corresponding discriminative or backward model by

$$W_x X = \hat{S}_x. \tag{2}$$

Here, $A_x \in \mathbb{R}^{N_x \times K_x}$ is the mapping matrix and $W_x \in \mathbb{R}^{K_x \times N_x}$ is the demixing matrix that extracts the estimated latent factors \hat{S}_x . In general, the linear forward model can additionally contain the noise term $\epsilon_x \in \mathbb{R}^{K_x}$ capturing activity that is not explained by the K_x components. In our approach, we consider the noiseless model for ICA. Here, the effect of noise can be mitigated through order selection in overdetermined cases (Li et al., 2007; Fu et al., 2014b) or another stage of decomposition (in our approach using CCA). Table 1 summarizes the notation used in this manuscript. For more details on the interpretation of linear models in multivariate neuroimaging, please refer to (Haufe et al., 2014).

Since without additional constraints the factorization of A and S is not unique, further assumptions about spatial and temporal dynamics are required for BSS. These distinguish different approaches and their suitability for application to fNIRS signals. A powerful way to obtain a unique decomposition under very relaxed conditions is through the assumption of statistical independence of the latent variables in the linear mixture, and when both sample dependence and higher-order statistics are taken into account, ICA can even estimate multiple Gaussian sources (Adali et al., 2014).

The mutual information framework for ICA. The goal of ICA is to find a demixing matrix W that yields maximally independent source estimates



NC1: Environmental influences	e.g., ambient light changes
NC2: Instrumentation noise	e.g., drifts, electr. interference, thermal /shot noise level shifts
NC3: Acquisition geom. changes	e.g., optode shifts rel. to each other or the scalp
C6: Systemic activity	e.g., HR, RESP, MW, VLFO
C5: Systemic activity	e.g., HR, RESP, MW, VLFO, non-evoked hemodynamics or vasomotion
C3: Systemic activity	Changes in blood pressure, skin/scalp blood flow / volume
C2: Systemic activity	Changes in blood pressure, CBF/CBV and PaCO ₂ , hypo-/hypercapnia
C4: Spontaneous brain activity	Non-evoked neurovascular coupling due to resting state activity
C1: Functional brain activity	Evoked local neuronal hemodynamic response (neurovasc. coupling)

Fig. 2. Components in measured fNIRS signals. Evoked and non-evoked functional signals of interest (bottom) are often masked by physiological and non-physiological noise of equal or higher magnitude. We perform BSS to improve signal to noise ratio. HR: Heart Rate, RESP: Respiratory signals, MW: Mayer Waves, VLFO: Very Low Frequency Oscillations, CBF/CBV Cerebral Blood Flow/Volume, PaCO₂: Partial CO₂ Pressure.

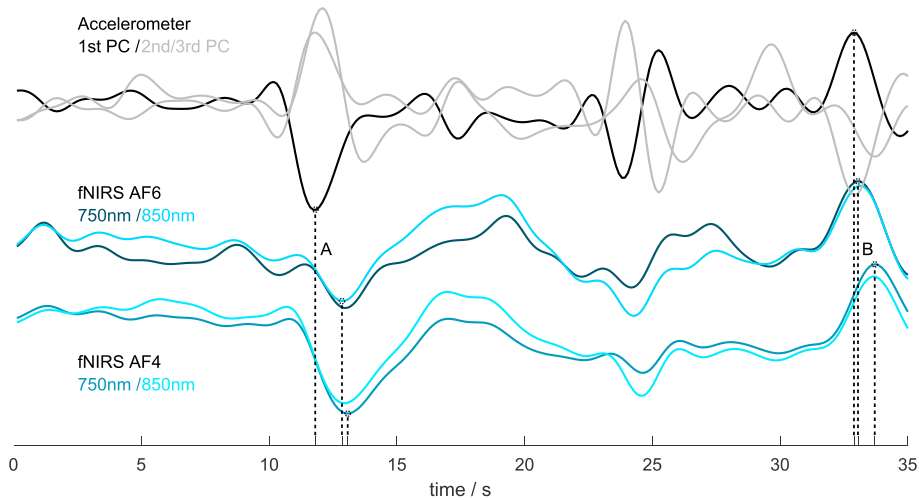


Fig. 3. Example of spatially dependent non-instantaneous and non-constant modulation of raw fNIRS intensity signals (AF4/AF6) in motion and first three PCA components of simultaneously acquired accelerometer on the head. Signals normalized and low-pass filtered with $f_c = 0.5$ Hz. Peak-to-peak delays: $A_{min|max} = 1050|1280$ ms, $B_{min|max} = 120|780$ ms.

\hat{S} . For the framework in this manuscript, we include the sample dependency of the sources in the ICA formulation. For this, a natural way to estimate \mathbf{W} is by the minimization of the mutual information rate which is given by (Adali et al., 2014)

$$I_r(\mathbf{W}) = \sum_{n=1}^{N_s} H_r(\hat{S}_n) - \log|\det(\mathbf{W})| - H_r(\mathbf{x}), \quad (3)$$

where H_r is the (differential) entropy rate. The cost function (3) takes both higher order statistics (HOS) as well as sample dependency into account.

Among the widely used ICA algorithms, Infomax (Bell and Sejnowski, 1995), uses a fixed nonlinearity model for the underlying distribution of the sources. ICA-EBM (Li and Adali, 2010) provides flexible density matching through the use of four measuring functions based on the maximum entropy principle and has been shown to maximize statistical independence efficiently. Most ICA algorithms take advantage of only higher-order statistics by ignoring sample dependence that exists in many signals — and certainly in fNIRS as well — by assuming independent and identically distributed samples. ICA-ERBM (Fu et al., 2014a) builds on the flexible density model of ICA-EBM and adds the use of sample dependence in addition to HOS to achieve ICA. By calculating the entropy rate of the sources in ICA-ERBM, and therefore taking advantage of multiple statistical properties, we expect to achieve a superior estimation of underlying sources in the presence of source dependence. We provide a brief overview on ICA-ERBM in the supplementary material 5.1.

Table 1
Notation.

$T_{x/z}$	Number of data points in modality x/z
$N_{x/z}$	Number of channels in modality x/z
Λ_x	Number of wavelengths per optode C_x in modality x
$K_{x/z}$	Number of latent factors (sources/components)
$\mathbf{x}_n / \mathbf{x}(t)$	T_x/N_x -dimensional row/column vector of observed data in modality x , here NIRS
$\mathbf{z}_n / \mathbf{z}(t)$	T_z/N_z -dimensional row/column vector of observed data in modality z , here Accelerometer
\mathbf{X}, \mathbf{Z}	$N_{x/z} \times T_{x/z}$ matrix containing the observed data in modality x/z
$\mathbf{s}_{x/z}(t)$	$K_{x/z}$ -dimensional vector of (estimated) latent factors of modality x/z
$\hat{\mathbf{S}}_{x/z}(t)$	
$\mathbf{S}_{x/z}, \hat{\mathbf{S}}_{x/z}$	$K_{x/z} \times T_{x/z}$ matrix containing all (estimated) latent factors of modality x/z
$\mathbf{A}_{x/z}$	$N_{x/z} \times K_{x/z}$ matrix of sensor-space patterns in forward models
$\mathbf{W}_{x/z}$	$N_{x/z} \times K_{x/z}$ matrix of filters in backward models

Canonical Correlation Analysis and temporal embedding. A method for finding co-modulating components in multivariate data is Canonical Correlation Analysis (CCA) (Hotelling, 1936), see (Anderson, 1958) for a review. It estimates normalized linear filters $\mathbf{w}_x \in \mathfrak{N}^{N_x}$ and $\mathbf{w}_z \in \mathfrak{N}^{N_z}$, the canonical variates, that maximize the canonical correlation between the projections of each modality:

$$\max_{\mathbf{w}_x, \mathbf{w}_z} \text{Corr}(\mathbf{w}_x^T \mathbf{x}(t), \mathbf{w}_z^T \mathbf{z}(t)). \quad (4)$$

If the two modalities do not correlate instantaneously, optimal filters depend on an — usually unknown — time lag τ . One solution is to temporally embed one modality with a given set of D time lags $\{\tau_0, \dots, \tau_D\}$, thus optimizing time-lag-dependent projections

$$\max_{\mathbf{w}_x, \mathbf{w}_z(\tau)} \text{Corr} \left(\sum_t \mathbf{w}_x^T \mathbf{x}(t), \mathbf{w}_z^T(\tau_i) \mathbf{z}(t - \tau_i) \right). \quad (5)$$

This method has been applied to medical imaging in various forms, for instance with kernel CCA for multimodal fMRI analysis (Bießmann et al., 2009), or without temporal embedding in fNIRS (Caicedo et al., 2013).

2.4. Time embedded multimodal BSS approaches for fNIRS

In our approach, we tackle the challenge of fNIRS signal decomposition by exploiting the combined strengths of the aforementioned linear methods. In a first step, we decompose the fNIRS signals into mutually independent sources with ICA-ERBM, taking sample dependency and HOS into account. Performing further analysis and processing steps in the source space then allows to increase the distance between components of interest and components for manipulation and rejection. Employing CCA, we exploit target signals from an additional modality, allowing the identification and extraction of co-modulating components. To take care of non-instantaneous coupling dynamics, the complementary target signal is temporally embedded.

In the context of direct and indirect movement artifact rejection, the application of accelerometer signals as targets is a natural choice. In the following, we describe BLISSA²RD, one possible implementation for the rejection of (indirect) movement artifacts based on the proposed framework.

BLISSA²RD: Blind Source Separation and Accelerometer based Artifact Rejection and Detection. To increase the SNR of cerebral neuronal components of interest in the fNIRS signals, we make use of the backward ICA-ERBM model in conjunction with multimodality and CCA by assuming that

fNIRS and accelerometer data sets are related by pairs of shared processes whose components BLISSA²RD aims to extract and reject.

Fig. 4 gives an overview of the method, Fig. 10 in subsection 3.0.1 complements this description with typical signals observed in the different stages of BLISSA²RD.

In a preprocessing step, both the fNIRS data X and accelerometer data Z are channel-wise normalized to zero mean and unit variance, then linearly detrended and low-pass filtered with a cut-off frequency of $f_c = 0.5$ Hz. We use a comparably high cutoff frequency at this stage for better separability in the following process and apply conventional processing steps, including a low-pass with a lower cutoff after cleaning. The accelerometer signals, usually acquired at sample rates higher than fNIRS (here 50 Hz), are then sub-sampled to a common time base using linear interpolation and a polyphase anti-aliasing filter.

In the fNIRS domain, we pool all wavelengths in X and perform ICA unmixing of the raw fNIRS intensity signals with ICA-ERBM (Fig. 10 I). For this, a hyperparameter, the filter length p_{fl} has to be selected. Its value determines the number of samples included in the whitening process of ERBM (Fu et al., 2014a). We do not elaborate its selection further in this manuscript but provide a brief note in the supplementary material 5.2.

On the accelerometer data, Principal Component Analysis (PCA) is performed for dimensionality reduction to $K_z = 3$ pairwise orthogonal Euclidean dimensions by selecting the three components with highest eigenvalues. This step is redundant when only one 3D accelerometer on the head was used for the acquisition of movements. By appending D time-shifted copies of the original (PCA reduced) data $S_z(\tau_d)$, the three main movement components are then temporally embedded into a higher dimensional space (Fig. 10 II) to take non-instantaneous coupling into account: $\tilde{S}_{z,z} = [S_{z_0}, S_{z_1}, \dots, S_{z_D}]^T \in \mathbb{R}^{DK_z \times T_z}$.

For the time shifts $\tau_d = d \cdot \Delta t$, $d \in \{0, 1, \dots, D\}$ the number of copies D and step width Δt have to be set. The selection of these parameters impacts the effectivity of the method concerning the coupling between movement (accelerometer signals) and fNIRS components. We can include apriori knowledge of the physiological signal for this purpose: A)

Causality. Movement induced artefactual fNIRS components cannot precede the accelerometer signals: time-embedding only in positive directions. B) The fNIRS frequency band of interest limits the size and number of time shifts that are reasonable. Using the time-embedded main movement components $\tilde{S}_{z,z}$ and the factorized independent fNIRS components \hat{S}_x , we now perform Canonical Correlation Analysis (Fig. 4 & Fig. 10 III), finding projections U_x and V_z of both modalities that correlate maximally. On the fNIRS side, we assume n projections $u_{x,n} \in \mathbb{R}^{T_x}$ that exceed a canonical correlation threshold to be artefactual components caused by movements. Applying Theorem 1 in (Haufe et al., 2014), these are then projected back by the means of eq. (6) and subtracted from the independent fNIRS sources (Fig. 4 & Fig. 10 IV). Finally, back-projection of the cleaned fNIRS sources into the original intensity domain and reversing the normalization yields the raw fNIRS signals that are now cleaned from (time-delayed) processes that correlate with movement (Fig. 4 & Fig. 10 V).

$$A_x^{CCA} = \text{Cov}(\hat{S}_x) W_x^{CCA} \text{Cov}(U_x)^{-1} \quad (6)$$

2.5. Dataset: a new experimental paradigm

While a variety of new fNIRS application scenarios in more natural lifelike environments is on the horizon, there is still a lack of instruments, experiments and data sets (Shin et al., 2017, 2018) that allow the development and evaluation of methods in that domain. To alleviate this, we designed and performed an experiment for the multimodal acquisition of neurophysiological data to infer short time memory-based cognitive workload from freely moving participants performing modified spatial n-back tasks. The paradigm aims to constrain the participants only minimally while at the same time enabling a high control of experimental conditions under quasi-realistic circumstances.

For the miniaturized and wireless synchronous acquisition of fNIRS, EEG, 3D-accelerometer and other physiological signals, we made use of two of our recently developed hybrid M3BA modules (von Lüthmann

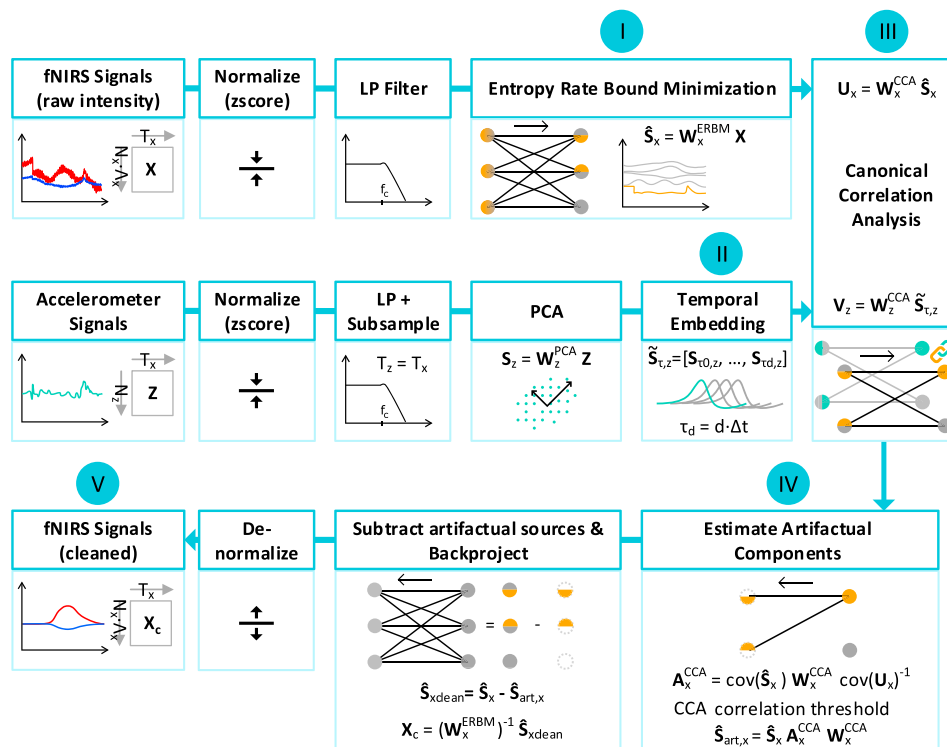


Fig. 4. BLISSA²RD Method Overview. I) ICA decomposition step, II) temporal embedding of principal accelerometer components, III) identifying shared processes with CCA, IV) estimating artefactual components in the ERBM source space, V) cleaned signal.

et al., 2017) in a wearable ultra lightweight fiberless headset (< 150 g, see Fig. 6). By the means of this novel fiberless instrumentation approach we achieved highly stable optical coupling between frontal optodes and the scalp, preventing optode shifts and resulting direct movement artifacts to the greatest extent in this study.

A Spatial color n-back paradigm in freely moving subjects. The overall set-up and basic protocol are depicted in Fig. 5 to elucidate the explanation of the following experiment.

A freely moving subject stands in front of a wall with 8 tiles equidistantly placed every 45° on a circle with an individually adjusted radius R . It is defined by the subject's height h with $R = 0.45 \times h$, which also approximates half of the span of outspread human arms. The center is located at the participant's solar plexus. Here, a screen shows instructions and visual cues.

The tiles are sized $10 \times 10 \text{ cm}^2$ and are illuminated in 8 different RGB states (red, magenta, blue, light blue, green, yellow, white, OFF). Pressing a tile activates a push button. In each of the 12 experimental blocks with a respective duration of 10 min, the participant performs a sequence of 7 rounds based on a modified spatial n-back task, alternating $n = 0$ with a pseudo-randomized order of $n = 1, 2, 3$. Each block starts with a resting period of 30 s. At the beginning of each round, an instruction cue is shown on the screen for 6 s. In this time, a pseudo-randomized target color (all RGB states except OFF), the constant default color OFF and the n-back instructions are displayed. 0-back rounds consist of 6 trials; 1,2,3-back rounds consist of 18 trials, each with constant duration of 6 s. At the beginning of each trial, the color configuration is instantaneously and pseudo-randomly reconfigured; each tile has a unique color. The participant has to decide for, and press one of the eight tiles within each

trial and selection speed is not rewarded. For motivation, correct selections add points to a block-wise score, erroneous/or no selections within the trial period lead to a small penalty. The target color and n-back level define the task to solve in each trial to follow in the same round. See also Fig. 5 for examples:

- In 0-back, the target and default colors are both OFF. In each trial, the subject finds and selects the only tile that is not illuminated. There are $n = 0$ positions to memorize. This serves as a baseline task.
- In $n = 1, 2, 3$ - back, a tile is to be selected whenever the target color reappears in $n + 1$ subsequent trials on the same spatial location. If this condition is not met within a trial, the tile with the default color OFF has to be pressed. In each trial, the participant has to remember and mentally update the target color position of $n = 1, 2, 3$ preceding trials.

Only 25 % of $n = 1, 2, 3$ - back trials and all 0-back trials within each round fulfill the target condition. Speakers provide simple auditory cues for rewards, penalties and the begin and end of each trial. Participants were instructed to use only their dominant hand for all button presses. After each block, there was a 3 min pause, after every 4th block a break of arbitrary individually chosen length. The experiment was performed with 17 + 11 participants (16 female, 27 right-handed), with age $28.1 \pm 5.8 \text{ y}$ and height $172 \pm 9.4 \text{ cm}$ (mean±std). 11 participants took part in a preliminary study with a slightly different protocol (less but longer blocks) but same paradigm and randomization. The experiment was conducted in accordance with the declaration of Helsinki and approved by the Ethics Committee of Berlin Institute of Technology (approval

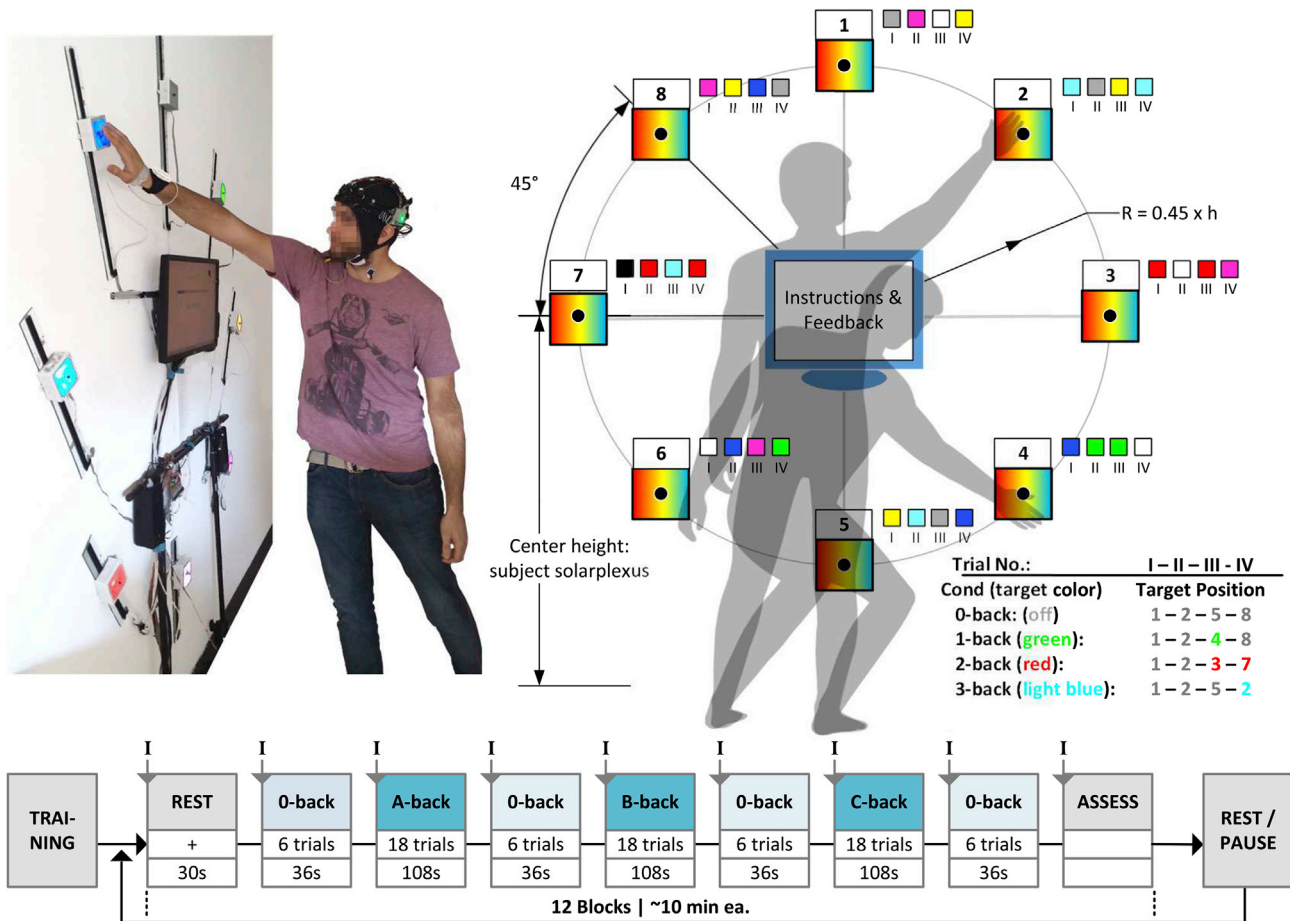


Fig. 5. Spatial n-back based cognitive workload paradigm with freely moving subjects. A,B,C: placeholders for pseudo-randomized sequence of 1,2,3-back task. Small colored squares next to tiles mark example configuration, roman letters mark number of the first four trials within an example round. “Target Position” given in the table marks the correctly selected position in each exemplary n-back task.

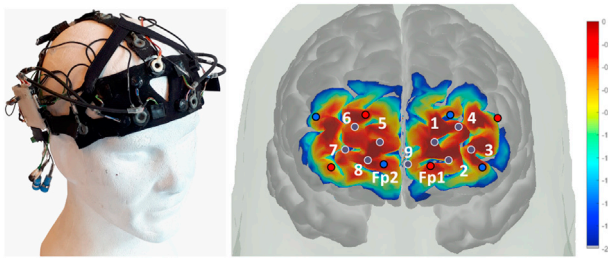


Fig. 6. (left) hybrid EEG-fNIRS headset. (right) fNIRS channel placement and sensitivity map. Red: emitters, blue: detectors, black: measurement channels. Visualization with Homer2 Atlas Viewer (Huppert et al., 2009).

number: LUE_01_20161117). All participants had normal or corrected to normal vision, and none of the participants reported color-blindness or neurological, psychiatric, or other brain-related diseases. All participants were informed about the experimental procedure, anonymized data evaluation, and distribution, and gave written consent prior to the experiment. The fNIRS optodes used in this study were placed on the forehead with a source-detector separation (SDS) of 30 mm and with the frontmost optode pair registered to the EEG 10–20 positions *Fp1* / *Fp2*, resulting in 9 channels over left and right superior-, medial- and medial-orbital -frontal regions, see Fig. 6. Signals were sampled at a rate of 8.33 Hz. X,Y,Z-accelerometer data was acquired at 50 Hz by both M3BA modules, which were rigidly incorporated into the headset between the pre-auricular and parietal points P7/8 respectively.

While the task difficulty is modulated by the number of positions that have to be memorized and mentally updated in each trial, all other experimental conditions remain constant regardless of the task and individual performance. This includes trial duration, color and spatial randomization and one performed selection in each trial. Individualized tile distances lead to equal movement conditions and well defined terminating postures across all participants and enforce stepping forward/backward for full vision and access to the field. While the trial length of 6 s leads to a shared frequency band between artifacts and hemodynamic responses, the overall block-lengths also enable analysis of slower fNIRS signal changes.

2.6. Evaluation metrics

A general challenge in the evaluation of motion artifact rejection techniques in fNIRS signals is that the ground truth is lacking, as the true hemodynamic response is unknown (see also (Brigadoi et al., 2014)). Here, we present the methods and metrics employed for quantitative evaluation based on statistical signal properties, target signals from multimodality, physiological plausibility, simulations and comparison of performance with established methods. We evaluate on the 17×120 min dataset from the experimental main study. As common preprocessing step, we linearly detrend channels to remove slow drifts and then apply a 4th order zero-phase Butterworth low-pass filter with $f_{c1} = 0.5$ Hz. This first filter stage improves BSS performance as it limits the decomposition to components in the bandwidth of interest. BLISSA²RD artifact rejection is always performed block-wise. Signal bandwidth is further reduced ($f_{c2} \in \{0.2, 0.033\text{Hz}\}$) as a last common step. Statistical tests employed for significance are paired t-tests.

2.6.1. Assessment: Blind Source Separation of fNIRS signals

Qualitative Investigation. The practical success of unmixing real-world fNIRS signals with BSS methods depends on the quality of decomposition achieved by the applied ICA approach. We focus here on the comparison of ICA-ERBM and popular FastICA (Hyvärinen, 1999). Decomposition quality was assessed visually with respect to separability of components, using apriori knowledge about

- (1) causal dependencies between time logged events, movement artifacts, and complementary accelerometer signals and
- (2) morphology, smoothness and discriminability of commonly known physiological components in fNIRS such as the pulse wave or LFOs (see Section 2.1).

ICA enables unique identification of the underlying sources under very general conditions (Adali et al., 2014; Comon and Jutten, 2010). Estimated sources of different ICA algorithms from the same data are ambiguous with respect to permutation and scaling (Comon and Jutten, 2010; Hyvärinen et al., 2004). Alignment of sources was performed using Bertsekas auction algorithm (Bertsekas, 1988; Rodriguez et al., 2014; Boukouvalas et al., 2018a,b) (one-sided, fixed epsilon) in the normalized FFT domain.

Simulated Data and Decomposition Metrics. In a simplified approach, we simulate fNIRS source characteristics to quantify some of the concerns raised in section 2.2 and to complement the qualitative inspection. 7 processes are generated for $t \in 0 \dots 100$ s, sampled at $f_s = 8$ Hz (see Fig. 15 and Supplementary Material 5.3), representing S_1) Breathing, S_2) Heart rate, S_3) Mayer waves, S_4) Evoked responses, S_5) White random gaussian noise, S_6) Movement artifacts and S_7) Dependent evoked processes.

Two pairs of sources are statistically dependent: S_1 and S_2 are weakly correlated (< 0.1) and S_4 and S_7 are moderately correlated ($\mu \pm \sigma = 0.39 \pm 0.23$, see also Fig. 9 B). While sources $S_1 - S_4$ remain constant, $S_5 - S_7$ are newly generated in each iteration. Observations are generated with a constant, arbitrary mixing matrix A and subsequent unmixing is performed with ERBM and fastICA. As before, estimated sources from each method are aligned to their corresponding ground truths using Bertsekas auction algorithm in the normalized FFT domain. To quantify unmixing performance, two metrics are investigated: Intersymbol interference (ISI) as a global metric, and the correlation between aligned estimated and true sources: $\text{Corr}(\hat{S}_i, S_i) \mid i \in \{4, 7\}$. ISI is a performance index, also known as Amari Index, measuring the quality of separation for BSS algorithms and is invariant to source scaling and permutation (Macchi, 1993; Choi et al., 2003; Eriksson and Koivunen, 2004; Long et al., 2018). Simulations are repeated $N = 1000$ times. To better differentiate the ISI results, convergence/stability of the unmixing performance is assessed as follows: Let $G = WA$ with W the estimated demixing matrix and A the true mixing matrix. The unmixing is considered stable, if the locations of the largest squared elements in any two rows of G are different.

2.6.2. BLISSA²RD performance: extraction of artifacts

Although the ground truth is unknown, essential features of task-related hemodynamic responses are by now well understood and typically stable. Commonly, averages are calculated, and the variability between single trials is assumed to be caused by the non-evoked processes of both systemic origin and motion artifacts. Ideally, the evoked neuronal response in a single subject should be stationary across rounds of the same cognitive task. In contrast, when averaging across many trials with constant movement conditions (here selected tile position), the induced hemodynamic motion artifacts should be stationary to a high degree. Under this assumption, we use 1st and 2nd order statistics for investigation of average artifacts and SNR:

Average Artifacts in the Chromophore Domain. Over the course of the whole experiment, each participant performed approximately 930 time-logged, randomly distributed button presses. We determine the average induced hemodynamic artifacts from 113 signals each, for all end-positions and all channels, both within and across subjects: fNIRS signals are segmented into epochs of ± 3 s around each button-press event; we then calculate averaged hemodynamic artifacts for HbO/HbR in each movement condition, channel, and subject, a total of $2 \times 8 \times 9 \times 17 = 2448$. We do this for both the original data and the data cleaned with BLISSA²RD. As the average artifact-free signal is expected to be

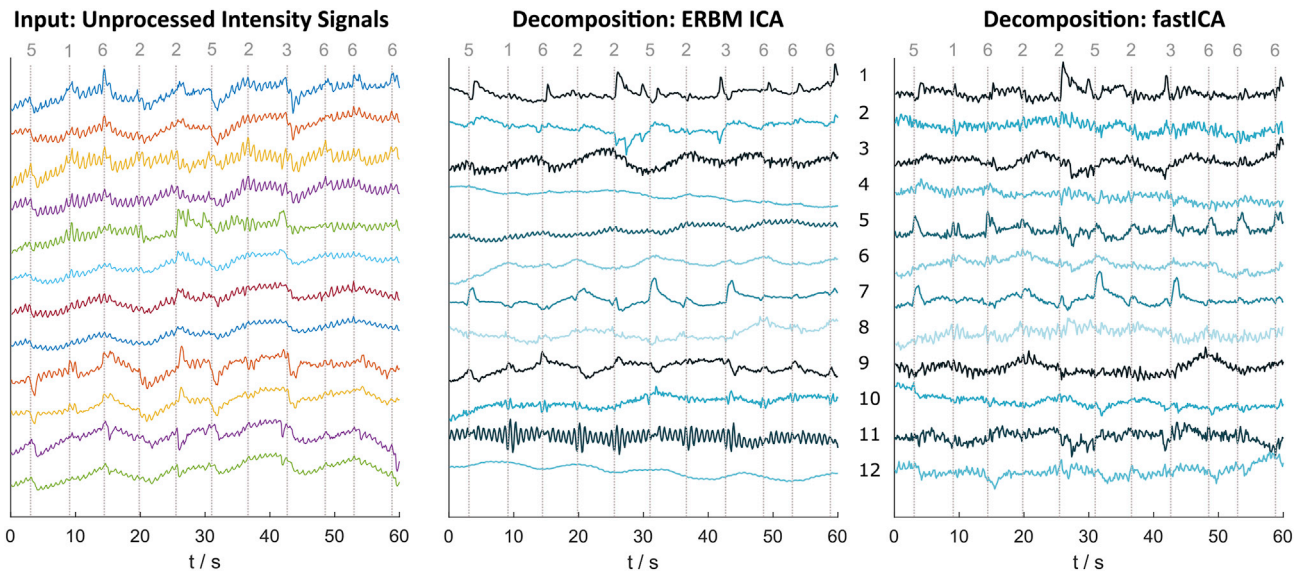


Fig. 7. Source separation in fNIRS. **(left):** Unprocessed raw intensity signals from the experimental dataset as input to ICA decomposition. **(mid, right):** 12 aligned components resulting from ERBM ICA (**mid**) and fastICA (**right**). ERBM ICA results in smoother and more distinguishable components from movement artifacts (1,2,7,9) pulse wave (11) and Mayer waves (12). Grey dotted lines indicate button-press events in the experiment, grey numbers the corresponding position, resulting in DMA (see also Figs. 5 and 11 for reference).

constant and close to zero, we make use of the peak to peak amplitude A_{pp} and the standard deviation of the average signal across time $\bar{\sigma} = \text{std}(\mu(t))$ in each channel to quantify average artifacts in each position before and after cleaning.

Within-Subject Standard Deviation/SNR of Slow Task-Related Hemodynamic Signals. The majority of conventional fNIRS studies aim to extract task-related hemodynamic response functions (HRFs) using an fMRI inspired supervised (canonical) GLM regression approach and often block averaging. This analysis typically requires a study design with repetitive and known stimuli in the order of 10 s. In contrast, the paradigm in this study aims to evoke signals suitable for unsupervised long-term monitoring and discriminating working memory load under realistic circumstances: While single trials within each block are 6 s long and provide a stimulus each, the mental tasks and induced responses depend on the continuous effort across trials within 90 s rounds. Consequently, we focus on slow (long term) fNIRS signal trends in the following. For each subject and experimental n-back condition ($n \in \{1, 2, 3\}$), the signals are segmented into $P^n = 12$ epochs using the first 90 s of each round. The same metric $\bar{\sigma}$ denoted “within-subject standard deviation” in (Brigadoi et al., 2014) is being used as a measure of noise in the evoked

physiological HbO/HbR signals: $\bar{\sigma}$ is the mean between-epoch variability of hemodynamic responses: The standard deviation across epochs P^n of the mean across time of the same condition n . It is assumed as an approximation that the stationarity of the evoked physiological hemodynamic response μ_{hrf} prevails, while the variability between single epochs of the same condition $\bar{\sigma}$ is predominantly due to motion artifacts. We then quantify the channel-wise improvement of SNR achieved by our cleaning approach by

$$\begin{aligned} \Delta\text{SNR} &= \text{SNR}_{\text{clean}} - \text{SNR}_{\text{orig}} \\ &= 10\log_{10}\left(\frac{\mu_{hrf}}{\bar{\sigma}_{\text{clean}}}\right) - 10\log_{10}\left(\frac{\mu_{hrf}}{\bar{\sigma}_{\text{orig}}}\right) = 10\log_{10}\left(\frac{\bar{\sigma}_{\text{orig}}}{\bar{\sigma}_{\text{clean}}}\right) \end{aligned} \quad (7)$$

Noise and SNR improvement are determined in $17 \times 3 \times 9 \times 2$ (subj \times conditions \times ch \times HbO/HbR) = 918 average slow prefrontal oxygenation signals, each from 12 experimental runs in the same n-back condition over the course of 90 s.

2.6.3. Comparison of BLISSARD performance: recovery of simulated HRFs

In the following, we present the methods applied for a comparison

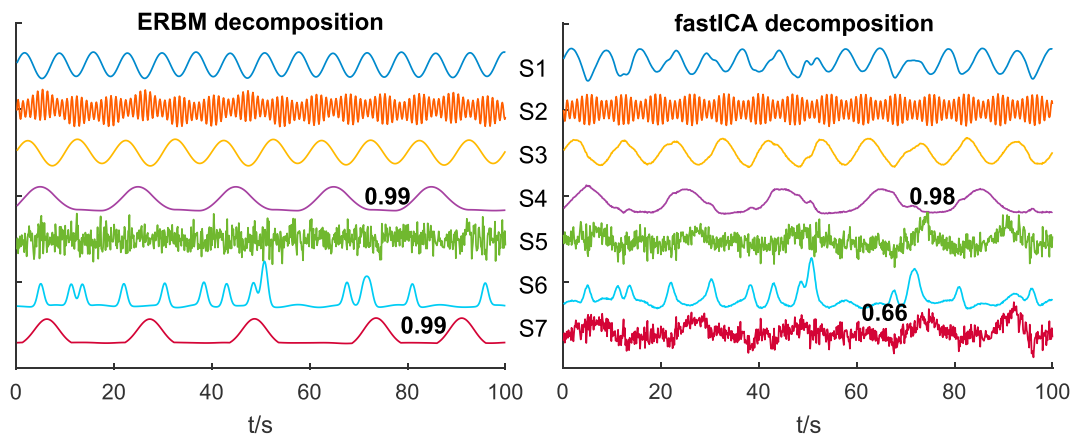


Fig. 8. Typical example of simulated fNIRS data unmixed with ERBM-ICA and fastICA. Sources representing breathing (S1), heart rate (S2), Mayer waves (S3), evoked responses (S4), white noise (S5), movement artifacts (S6) and dependent evoked processes (S7). Bold numbers: correlation between ground truth and estimated sources.

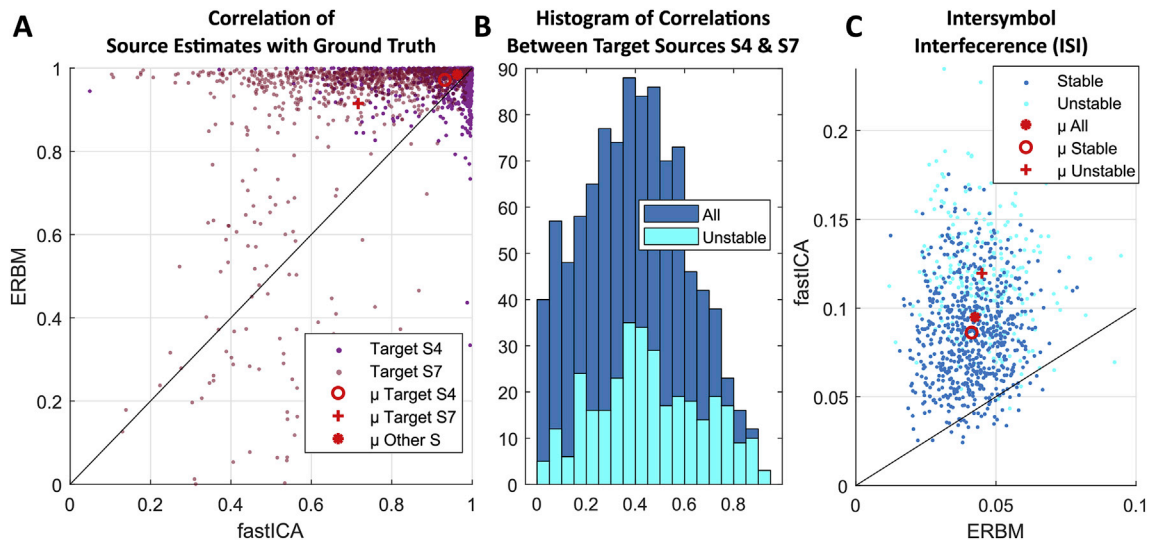


Fig. 9. Results of fNIRS source (un-)mixing simulation in 1000 iterations. (A) correlation of true sources S_4 & S_7 with source estimates from ERBM/fast ICA. (B) histogram of correlation between true target sources S_4 & S_7 in all iterations and fraction of corresponding unstable unmixing in fastICA and ERBM ICA. (C) Intersymbol interference (ISI) of ERBM ICA and fastICA.

between BLISSA²RD and three established algorithms for movement artifact removal. This enables a comparative assessment of its performance in conventional extraction of HRFs, as performed in (Brigadoi et al., 2014).

Simulated HRF on Real-World Data and Metrics for Quality Assessment. The real-life oriented spatial cognitive workload paradigm in this study provides comparatively long task periods and hemodynamic trends, and no ground truth. A straight-forward conventional approach is therefore not feasible. Instead, as a remedy, we simulate known ground truth HRF onto the real fNIRS data from 1-back tasks. These provide realistic movement artifacts and physiological signals, while the continuous hemodynamic trend due to the ongoing low mental effort is still rather weak. We split each 90 s long 1-back round after the instruction period into three non-overlapping 30 s windows. We then augment the raw intensity signals of a subset of 4 out of 9 channels within each window with a known prototypical HRF (total length 18 s, see Figure 13, black signal), starting at a normally distributed random offset between 0 – 10 s. This yields 36 HRFs in each augmented channel and participant, a total of 2448. Finally, the known ground truth HRFs and the augmented data are used for performance evaluation on the basis of two performance metrics: (1) the Pearson correlation (PCorr) and (2) the Root Mean Square Error (RMSE) between the ground truth and extracted HRF after artifact rejection.

Analysis Pipeline for Comparison with PCA, Spline and Wavelet Approach. For a better overall comparability, we follow the same processing pipeline and parameter selection given in (Brigadoi et al., 2014), using HOMER2 toolbox functions (Huppert et al., 2009) for all processing steps and conventional artifact removal. With the above performance metrics, we compare BLISSA²RD with established PCA, Spline and Wavelet approaches. The processing and used parameters are follows:

1. Conversion from raw intensity data to changes in optical density (OD)
2. Removal of noisy channels
3. Motion artifact detection for PCA, Spline and Wavelet method [$t_{Motion} = 1.0$, $t_{Mask} = 1.0$, $AMP_{thresh} = 0.4$, $STDEV_{thresh} = 10$]
4. Motion artifact correction [I) PCA ($n_{SV} = 90$), II) Spline ($p = 0.99$), III) Wavelet ($iqr = 1.5$, $db5$ -wavelet), IV) BLISSA²RD ($p = 15$, $\Delta t = 0.36$ s, $D = 5$, $corr_thresh = 0.4$), IV) no correction]
5. Bandpass filtering [0.01 – 0.5 Hz]
6. Conversion of OD to HbO/HbR concentrations using the mBLL
7. Subject wise block averaging (baHRFs) across all 36 trials of a channel.

8. Calculation of PCorr and RMSE between ground truth and baHRFs

In case of BLISSA²RD, we apply the same pipeline except that 5) and 1) are mutually exchanged: The method works best on intensity data, and source decomposition is improved when limited to the signal bandwidth of interest.

3. Results

3.1. Blind Source Separation of fNIRS signals

Qualitative Investigation: ICA of fNIRS Real-World Signals. Fig. 7 depicts a typical subset of aligned sources that were decomposed with ERBM ICA and fastICA from the same unfiltered raw intensity real-world fNIRS data. In the visual inspection, ERBM ICA consistently outperformed other tested ICA methods, yielding a higher number of unique and physiologically plausible and identifiable sources, e.g. from LFOs, pulse waves and movement artifacts, as well as generally smoother and less noisy shapes.

Performance Analysis: ICA of Simulated fNIRS Signals. The visual inspection is quantitatively complemented by the simulation results. Fig. 8 shows a typical example of simulated fNIRS after decomposition by ERBM ICA and fastICA. More details are provided in supplementary material 5.3.

ERBM ICA unmixing yielded 59 and fastICA yielded 290 unstable results out of 1000, where in 87 out of 290 cases fastICA did not converge to the correct number of 7 target sources. Fig. 9 A shows the correlation and ISI performance measures over all iterations of the decomposition performance analysis. In the following, we focus on the dependent target sources S_4 and S_7 , as these represent the evoked responses.

For target source S_4 , ERBM ICA yielded estimates that correlate with the true signal on average ($\mu \pm \sigma$) with 0.97 ± 0.04 , fastICA yielded 0.93 ± 0.10 . For the dependent target source S_7 , ERBM ICA yielded estimates that correlate with 0.92 ± 0.17 , where fastICA yielded corresponding estimates with 0.72 ± 0.19 . Across all other sources, the correlation is on average 0.98 ± 0.01 and 0.96 ± 0.03 for ERBM ICA and fastICA respectively. ISI analysis (Fig. 9 C) yielded an average ($\mu \pm \sigma$) ISI of 0.042 ± 0.012 in ERBM ICA and 0.095 ± 0.033 in fastICA for all decompositions. When only investigating unstable decompositions, ISI was found to be 0.045 ± 0.014 and 0.120 ± 0.033 respectively.

Exploiting Multimodality: Decomposition of fNIRS with BLISSA²RD. Following the formal description of each step in the multimodal

BLISSA²RD Processing Steps and Signal Domains

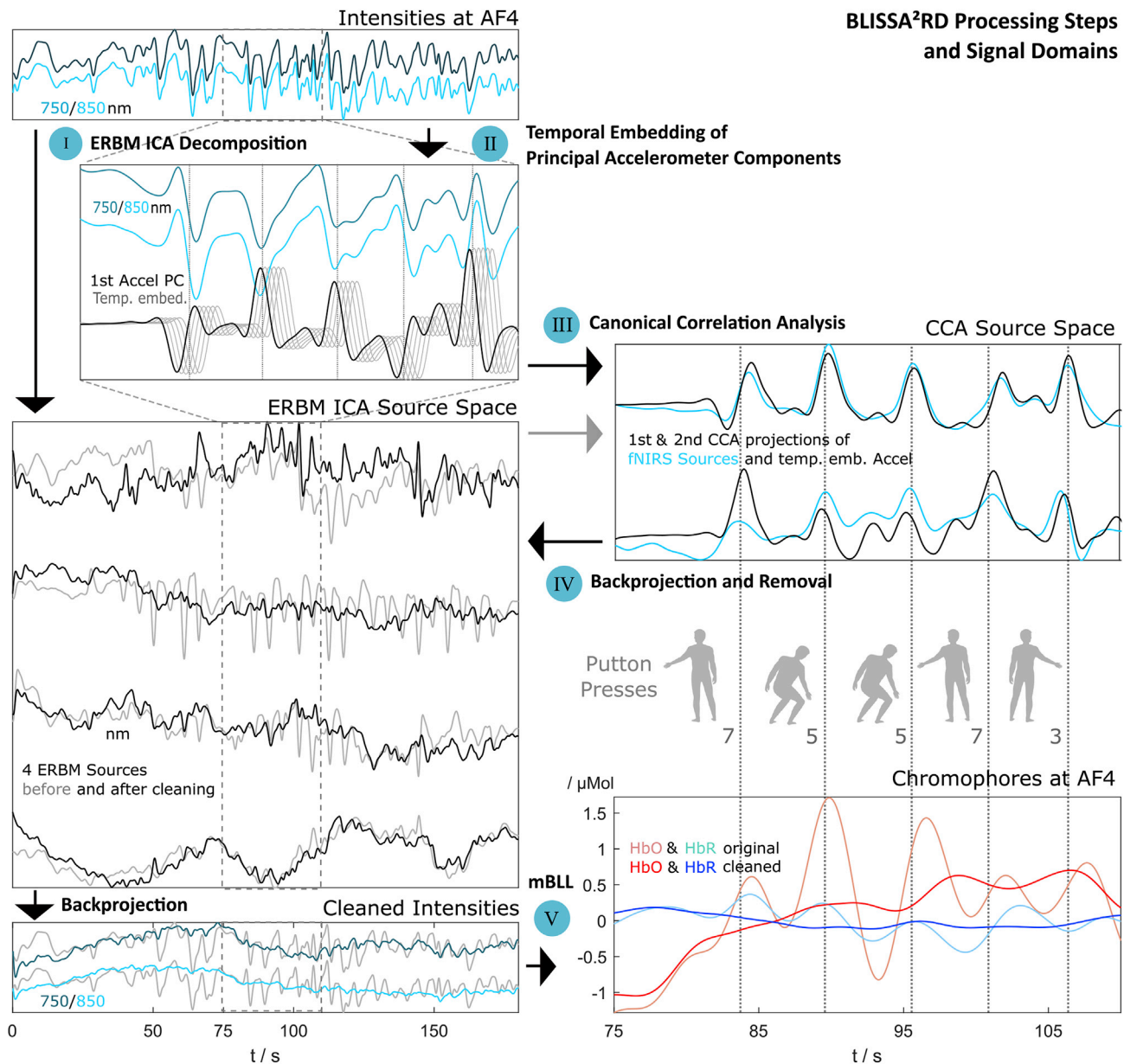


Fig. 10. Typical time series signals in different domains of BLISSA²RD, corresponding to steps in Fig. 4. Left side: 160 s time window, right side zoomed in at 75 – 110 s. Raw intensities of channel AF4 (upper left) and 4 exemplary sources after ERBM ICA decomposition before and after cleaning (I). Time embedded 1st principal accelerometer component with $\tau \in \{0, \dots, 1.8\text{ s}\}$ vs. raw signal (II) and first two resulting projections from CCA (III). Raw signals (lower left) and signals converted to chromophore concentrations before and after cleaning step (V). Grey dotted lines and numbers (right side) indicate button press events and positions in the experiment (compare Fig. 5). Input signals low-pass filtered at 0.5 Hz

BLISSA²RD approach in Figs. 4 and 10 exemplifies typical signals observed in the different domains of the method.

It illustrates amongst others that.

- ERBM ICA components are modulated by movements to different degrees - displayed before and after CCA artifact rejection step (10 I + IV).
- Temporal embedding of a principal accelerometer component (τ_D with $D \in \{0, \dots, 5\}$) helps to alleviate non-instantaneous coupling (10 II).
- CCA extracts shared processes from the ERBM ICA sources and temporally embedded principal accelerometer components with high canonical correlation (10 III, see also supplementary material 5.4).
- Signals before vs. after cleaning differ significantly in both the intensity and chromophore domain (10 V).

A quantitative investigation of co-modulation coefficients from cross-correlation analysis and BLISSA²RD CCA between accelerometer target signals and fNIRS signals is provided within the supplementary material 5.4. The choice and impact of the time embedding parameter τ is also discussed. On average, the first three extracted artifact components show a strong to moderate canonical correlation of 0.85 ± 0.06 , 0.71 ± 0.05 and 0.60 ± 0.05 for $\tau \geq 1.2\text{ s}$. For a suggested CCA threshold of 0.4, BLISSA²RD finds and removes on average 4 movement artifact components from the fNIRS time series data.

3.2. BLISSA²RD performance: extraction of artifacts

Average Artifacts in the Chromophore Domain, Fig. 11 A depicts the grand average hemodynamic artifacts in three exemplary channels AF3, Fpz and AF4 for all positions of the experiment and both the original and cleaned data. Average movement artifacts were each calculated from a

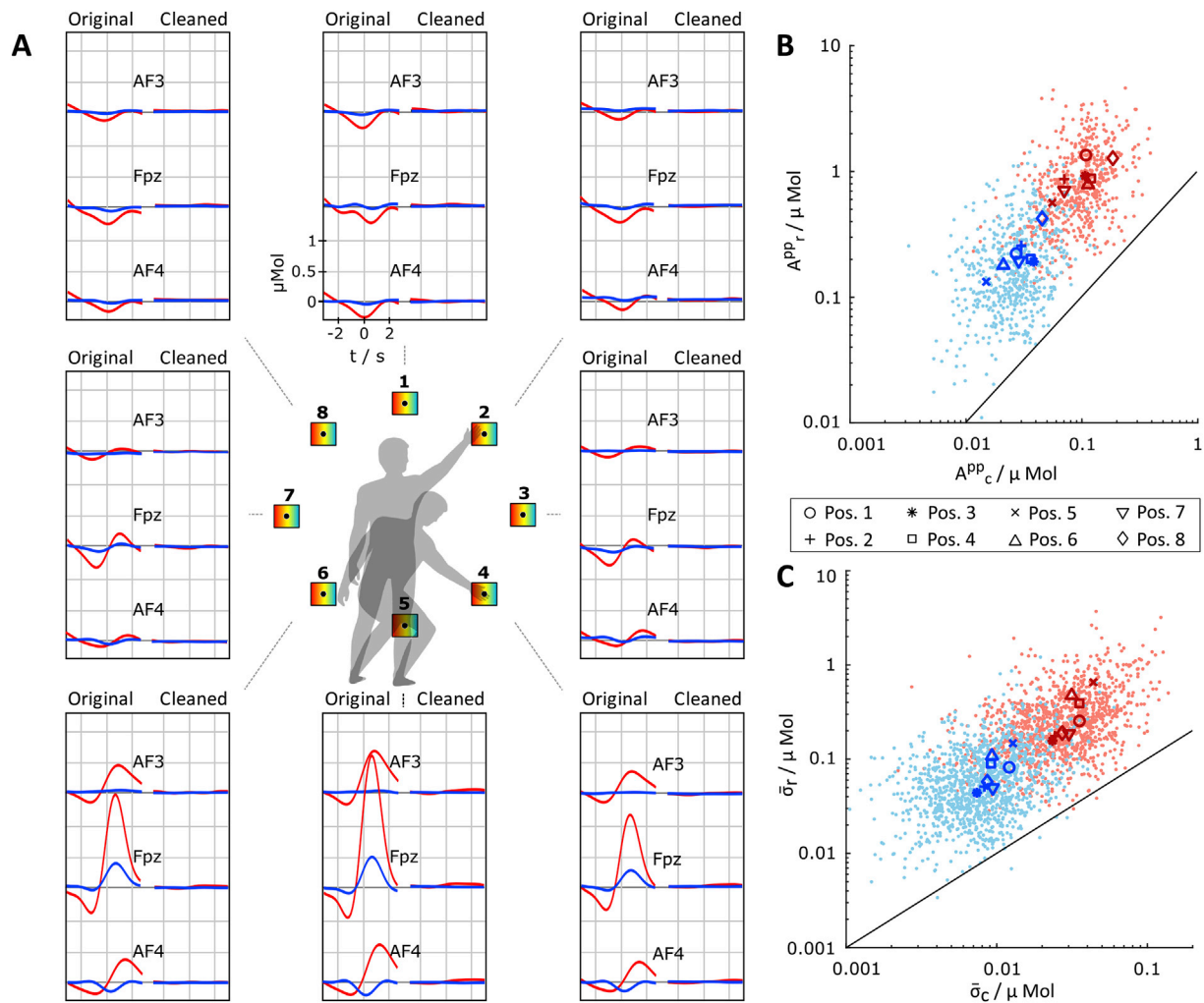


Fig. 11. Grand average hemodynamic artifacts and statistics. (A) Average signals for each button position in original data and data processed with BLISSA²RD of selected channels AF3, Fpz, AF4. Scatter plots of peak to peak amplitudes A^{pp} (B) and standard deviations σ^{μ} (C) of the average movement artifacts in each channel for each subject and position. Subscript “o” (y-axis): original data, subscript “c” (x-axis): cleaned data. HbO: red, HbR: blue.

total number of 1920 epochs across all subjects. In the unprocessed data, significant artifacts can be observed for all positions and channels (min. $0.2 \mu\text{Mol}_{pp}$ in HbO). Events where the participants stooped down (pos. 4–6) go along with largest changes (up to $3 \mu\text{Mol}_{pp}$ in HbO, up to $0.8 \mu\text{Mol}_{pp}$ in HbR in Fpz). Artifact morphologies differ between movement conditions but also between channels and often show an undershoot followed by a more substantial overshoot in HbO, where HbR can display a similar or inverse behavior. In positions above shoulder height (1,2,8), HbO typically displays only undershoots. In contrast, the data cleaned with BLISSA²RD, shows remaining average hemodynamic artifacts of max. $0.08 \mu\text{Mol}_{pp}$ in HbO and $< 0.01 \mu\text{Mol}_{pp}$ in HbR across all channels and positions, an attenuation of up to two orders of magnitude.

Scatter-plots in Fig. 11 B & C depict the peak to peak amplitudes A_c^{pp} / A_o^{pp} and standard deviations $\sigma_c^{\mu} / \sigma_o^{\mu}$ of the average hemodynamic artifact in single subjects, channels and movement positions for original (o) vs. cleaned (c) data. Across all subjects, channels and movement positions, application of BLISSA²RD reduces A^{pp} and $\bar{\sigma}$ of averaged hemodynamic artifacts in HbO and HbR on average by more than one order of magnitude and up to two orders of magnitude in subsets.

Within-Subject Standard Deviation/SNR of Slow Task-Related Hemodynamic Signals. Analysis of the within-subject standard deviation $\bar{\sigma}$ and SNR of original and processed physiological HbO/HbR signals during $n = 1, 2, 3$ -back tasks yielded the results summarized in Fig. 12 and Table 2.

Across conditions and subjects, for low-pass filtered signals with $f_c = 0.2 \text{ Hz}$, the within-subject standard deviation $\bar{\sigma}$ of the original signal is reduced on average by a factor 1.5 for HbO and a factor 1.3 for HbR through processing with BLISSA²RD. The SNR in each channel is improved on average by 3.64 dB for HbO and by 2.70 dB for HbR. For signals slower than 30 s with $f_c = 0.033 \text{ Hz}$, the improvement is on average still 1.75 dB and 1.61 dB respectively. As before, in channel and subject subsets, reduction of $\bar{\sigma}$ /SNR improvement are significantly higher up to factors around 3/ 10 dB. Fig. 12 C shows typical slow average hemodynamic signals at position AF6 across whole 90 s epochs of $n = 1 - 3$ conditions in an exemplary subject. In line with physiological expectations, an increased task difficulty (n) leads to an average HbO increase/HbR decrease over the whole time-course of each round. Within individuals, variability in average responses of the signals across trials is distinctly higher in original compared to cleaned data.

3.3. Comparison of BLISSA²RD performance: recovery of simulated HRFs

Fig. 13 shows results from the comparative block average HRF recovery performance analysis. The average correlations between recovered baHRFs and ground truth for all participants and channels is ($\mu \pm \sigma$ HbO/HbR): PCA ($.84 \pm .10 / .93 \pm .09$), Spline ($.83 \pm .13 / .89 \pm .13$), Wavelet ($.93 \pm .05 / .94 \pm .10$), BLISSA²RD ($.96 \pm .03 / .94 \pm .11$). The average root mean square errors (RMSE) between recovered baHRFs and

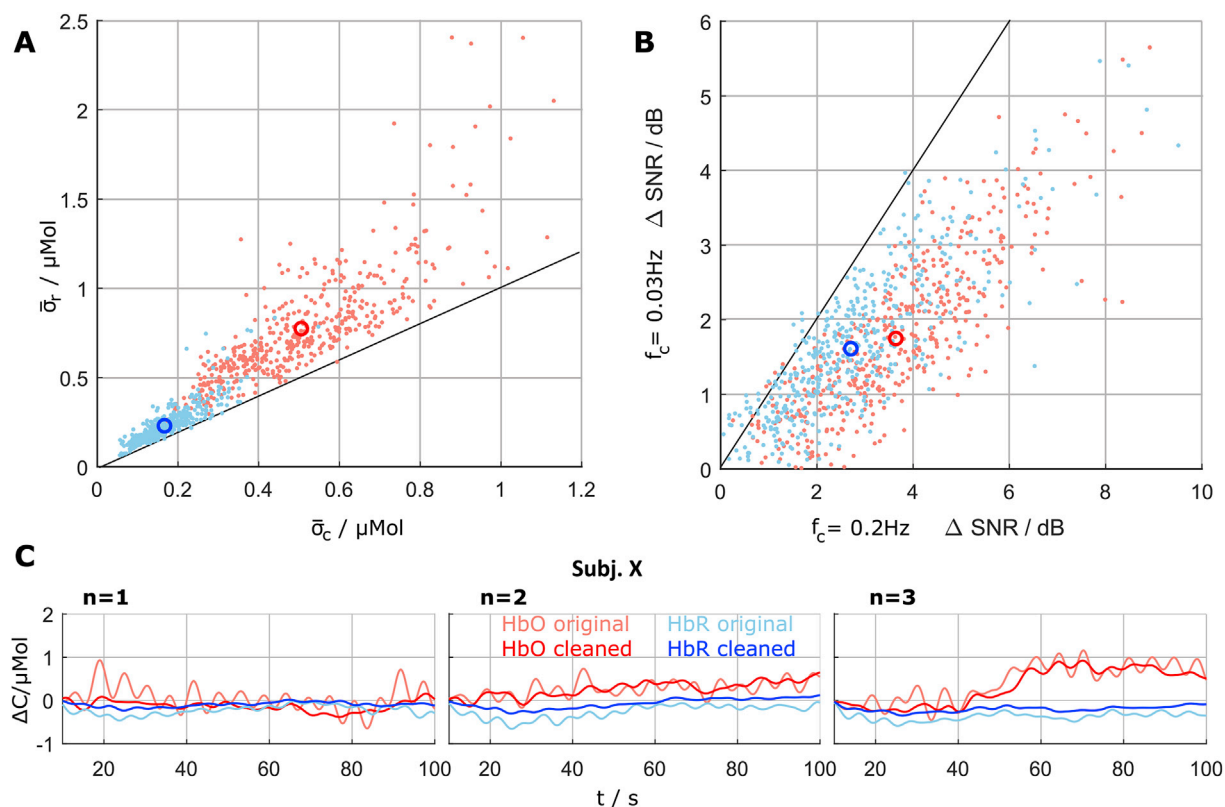


Fig. 12. A: Within-subject standard deviation of the original $\bar{\sigma}_r$ and cleaned $\bar{\sigma}_c$ signals. B: Scatter plot of SNR improvement across subjects and channels for normal ($f_c = 0.2$ Hz) and slow signals ($f_c = 0.03$ Hz). HbO: red, HbR: blue. C: Typical average slow hemodynamic signals of an exemplary subject in $n = 1 - 3$ conditions, $f_c = 0.2$ Hz, for both original data (HbO: salmon, HbR: sky blue) and cleaned data (HbO: red, HbR: blue) in channel AF6.

Table 2

Mean \pm std SNR improvement across all subjects and channels.

	n-back	Δ SNR /dB	Δ SNR /dB	Δ SNR /dB
		$f_c = 0.5$ Hz	$f_c = 0.2$ Hz	$f_c = 0.033$ Hz
HbO	1	4.58 \pm 1.99	4.10 \pm 1.81	1.83 \pm 1.13
	2	4.10 \pm 1.68	3.64 \pm 1.52	1.78 \pm 0.99
	3	3.60 \pm 1.78	3.17 \pm 1.62	1.64 \pm 1.14
HbR	1	3.50 \pm 2.03	3.01 \pm 1.76	1.80 \pm 1.08
	2	3.14 \pm 1.68	2.69 \pm 1.42	1.64 \pm 0.92
	3	2.88 \pm 1.77	2.41 \pm 1.47	1.40 \pm 0.99

ground truth are ($\mu \pm \sigma$ HbO/HbR): PCA (.35 \pm .18/.06 \pm .05), Spline (.41 \pm .32/.07 \pm .05), Wavelet (.17 \pm .10/.04 \pm .03), BLISSA²RD (.14 \pm .06/.05 \pm .03). In HbO correlation and RMSE, BLISSA²RD outperformed all other methods significantly (all $p < 0.01$ and below). In HbR correlation, except Spline, improvement was not significant. In HbR RMSE, BLISSA²RD outperformed PCA and Spline significantly (all $p < 0.01$ and below) and no significant improvement over the Wavelet approach was observed. All tests are paired t-tests.

4. Discussion and conclusion

We proposed an effective BSS framework and presented its implementation in the BLISSA²RD method for fNIRS signal decomposition, analysis, and movement artifact rejection. In the following, we discuss key findings and their implications.

fNIRS Blind Source Separation and ICA. ERBM ICA unmixing of real-world and simulated fNIRS data performed favorably over other tested ICA approaches that do not include both sample dependency and higher-order statistics. All methods performed better when applied to raw intensity signals compared to chromophores, which is consistent with expectations in linear models, due to the logarithmic nature of the modified

Beer-Lambert Law (mBLL). For a discussion of linear mixing and non-linearities, see also (Dähne et al., 2013). When decomposing intensity signals, it is essential to note implications for the interpretation of extracted latent factors and their link to the chromophore domain. We motivate the application of BSS with the separation into components that reflect independent physiological processes (e.g., Mayer Waves, pulse waves, motion artifacts, ...). However, the unmixing itself does not yield sources that can be interpreted physiologically without caution as such (see (Haufe et al., 2014)). In contrast, they are of information-theoretical origin and should be projected back to channel space, i.e., through eq. (6) (see also Fig. 4 E), for reliable physiological interpretation. Then, mBLL conversion to chromophores can be performed conventionally.

The qualitative results from visual inspection using real-world data were quantitatively confirmed by simulation results (see Figure 15). Decomposition performance was quantified with the correlation between estimated and true target sources and Intersymbol Interference of the estimated unmixing matrix. Due to the use of both HOS and sample dependence, ERBM ICA outperforms fastICA significantly in all metrics ($p \ll 0.001$) in the presence of source-dependence. As in the real-world data, this generally yields smoother and more distinguishable source components (e.g. Fig. 7).

Time embedding against non-instantaneous coupling and Canonical Correlation Analysis. By integrating time-embedded multimodal CCA into the proposed BSS framework, non-instantaneous and non-constant coupling between shared latent processes within fNIRS and accelerometer signals were successfully tackled. On average, BLISSA²RD identified and extracted up to 4 pairs of latent processes with a strong canonical correlation of up to 0.85, most substantially within time-embedding windows $\tau \leq 1.8$ s. These results appear to be also physiologically valid, as it is plausible that at least three Euclidean degrees of freedom in movement have a considerable impact on fNIRS signals. The approach also shows the importance of considering (co-)modulation delays in fNIRS signals

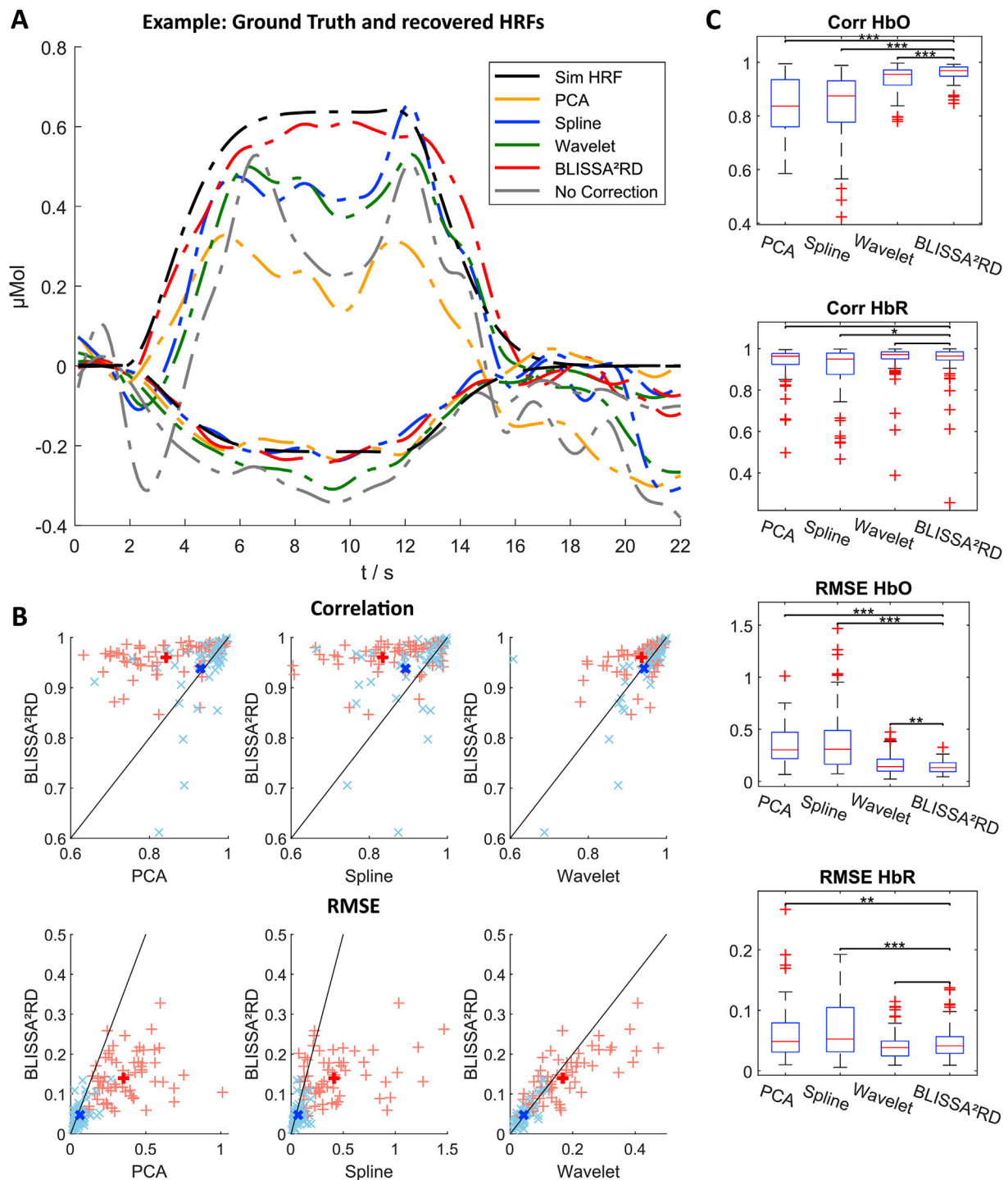


Fig. 13. Comparison of method performance in the recovery of ground truth HRF from highly contaminated real-world data. (A) Example of ground truth (black) and block average HRF (baHRF) recovered conventionally using different artifact removal methods. (B) Correlation and RMSE of recovered baHRFs vs. ground truth: BLISSA²RD vs other methods. Red: HbO, blue: HbR. Bold cross: mean. (C) Boxplots of median/std evaluation metrics for all methods. Stat. Significance: * $p < 0.05$, ** $p < 0.01$, *** $p < 0.001$.

and confirms its theoretically expected advantage over conventional cross-correlation analysis in the channel domain: This approach yielded only weak coefficients, noteworthy only for the first principal accelerometer component with ($\rho = 0.38$) on average (see supplementary material 5.4).

BLISSA²RD artifact rejection. The manifestation of indirect movement artifacts varies strongly between subjects, movement conditions, and particular channels. BLISSA²RD consistently performed well across all

factors: On average/in subsets, it attenuated hemodynamic physiological movement artifacts by one/up to two orders of magnitude, reduced the average within-subject standard deviation $\bar{\sigma}$ of slow evoked hemodynamic signals by a factor of 1.3/up to 3, and increased its SNR by 3.64 /2.70 dB (HbO/HbR)/up to 10 dB. Also for signals far slower than the semi-periodic movements ($f_c < 0.033$ Hz) improvement could be observed (1.75 /1.61 dB). Behavioral changes in body posture (e.g., a tilt of the head) and movement are likely the cause and indicate the

importance of approaches that consider indirect physiological movement artifacts beyond typically targeted optode shifts. The performance of BLISSA²RD was furthermore validated in a conventional stimulus-oriented HRF recovery approach using simulated HRFs as ground truth on the real-world data. For better comparability, we employed a well-established processing toolbox and signal processing pipeline and compared performance with three widely applied methods: PCA, Spline and Wavelet-based artifact rejection. These have also been evaluated with the same toolbox and pipeline in earlier works (Brigadoi et al., 2014). In both evaluation metrics, correlation and Root Mean Square Error to ground truth, BLISSA²RD outperformed all other methods significantly for HbO and performed comparatively or better than the other methods for HbR signals.

The results support the theoretical advantages of the proposed framework and show its potential benefit in both novel (mobile) long term monitoring approaches and fNIRS signal analysis, and as an additional preprocessing step in established conventional GLM regression based analysis pipelines in fNIRS. Although powerful statistical analysis tools come at the cost of higher computational complexity, the average runtime for cleaning a block of 10 min data (9 × 2 channels) in 2230 runs was still only 14 s on an intel i7vPro notebook with Mathworks Matlab2017b.

Limitations. BSS approaches require a minimum number of acquired channels to allow for stable decomposition into latent factors. For this reason, the proposed framework is not suitable in settings with very-low channel counts let alone single-channels. Single-channel artifacts, i.e., individual optode decoupling or shifts, will not reliably be rejected. These can, however, also be minimized by lightweight instrumentation, headset, and optode fixation designs and were observed only exceptionally in our M3BA-based (von Lüthmann et al., 2017) headset. The method's strength relies on the exploitation of both statistical independence between fNIRS sources and their co-modulation with movement signals - regardless of shared frequency bandwidth and signal dynamics. This strength depends on the validity of the assumption that evoked hemodynamic responses and physiological movement signals in the fNIRS channels are independent, which is typically true. However, exceptions are conceivable, for example when a movement-evoked artifact co-modulates with an evoked hemodynamic response in the corresponding sensory-motor region that was responsible for the movement itself. The analysis was performed on data recorded with a yet comparably low number of 9 optode pairs, which was found to be sufficient for the approach. Due to the inherent multimodality of BLISSA²RD, rigidly coupled accelerometer signals are a requirement that is currently not supported by the majority of commercial instruments, which may be an actual limitation when not using M3BA or alike. Similar to trends in wearable EEG, however, we expect wearable fNIRS to include accelerometers by default soon. Furthermore, the extension of any instrument with simple stand-alone accelerometer modules is fairly easily possible.

Outlook and further applications. The presented BSS framework is not limited to the analysis and rejection of artifacts and can easily be adapted to other purposes by exchanging methods and target signals, as the processing stages are modular. Possible expansions are A) performing ICA decomposition with TDSEP (Ziehe et al., 1998) to exploit time structure (pronounced autocorrelation) in the signals, when targeting at oscillatory physiological components. B) Applying Independent Vector Analysis (IVA) (Adali et al., 2014), the multivariate extension of ICA, which exploits dependencies between components as well as data sets. C) Using the temporally embedded CCA block as a superior approach to find optimal noise regressors for the conventional (canonical) GLM in fNIRS, e.g. by using short separation, accelerometer or other physiological auxiliary signals as inputs. We expect that the performance of BLISSA²RD can be further improved by expanding the degrees of freedom of provided movement target signals, e.g., by a combined accelerometer and gyroscope sensor. While accelerometer data as target signals for removal of motion artifacts are a natural choice, others can be used for

identification and analysis of co-modulating sources in the fNIRS time-domain. In the frequency domain, e.g., for EEG band-power features, other methods such as those of the SPoC family (Dähne et al., 2013, 2015; Fazli et al., 2015) are predestined.

The framework presented in this manuscript is a new type of multivariate methods for the BSS analysis of fNIRS signals and can be used as a blueprint for artifact rejection in complex environments beyond the applied paradigm. In combining strengths with existing complementary techniques such as multi-distance optode approaches, we see a promising way to achieve the robustness desired for new medical and research-oriented ambulatory neuroimaging applications.

BLISSA²RD is publicly available here: <https://github.com/avolu/BLISSARD>.

Declarations of interest

None.

Acknowledgments

AvL acknowledges support by the Berlin International Graduate School in Model and Simulation based Research (BIMoS). This work was also supported by the Institute of Information & Communications Technology Planning & Evaluation (IITP) grant funded by the Korea government (No. 2017-0-00451). KRM acknowledges partial funding by the German Ministry for Education and Research as Berlin Big Data Centre (BBDC) (01IS14013A) and Berlin Center for Machine Learning under Grant 01IS180371 and by DFG (EXC 2046/1, Project-ID 390685689). TA acknowledges support by the US National Science Foundation (grants NSF-CCF 1618551 and NSF-NCS 1631838). The authors thank Prof. Benjamin Blankertz, Stefan Haufe, PhD, and Andreas Ziehe, PhD for fruitful discussions of applied mathematical models, Stephanie Brandl and Daniel Miklody for help with manuscript revision, Prof. Gabriel Curio for discussing the design of the experimental paradigm and Marina González-Gómez for help with the graphical design of figures.

Appendix A. Supplementary data

Supplementary data to this article can be found online at <https://doi.org/10.1016/j.neuroimage.2019.06.021>.

References

- Adali, T., Anderson, M., Fu, G.-S., 2014. Diversity in independent component and vector analyses: identifiability, algorithms, and applications in medical imaging. *Signal Processing Magazine. IEEE* 31 (3), 18–33.
- Adali, T., Levin-Schwartz, Y., Calhoun, V.D., 2015. Multimodal data fusion using source separation: application to medical imaging. *Proc. IEEE* 103 (9), 1494–1506. <https://doi.org/10.1109/JPROC.2015.2461601>.
- Akgül, C.B., Akin, A., Sankur, B., 2006. Extraction of cognitive activity-related waveforms from functional near-infrared spectroscopy signals. *Med. Biol. Eng. Comput.* 44 (11), 945.
- Anderson, T.W., 1958. *An Introduction to Multivariate Statistical Analysis*, vol. 2. Wiley, New York.
- Andreu-Perez, J., Leff, D., Ip, H., Yang, G.-Z., 2015. From wearable sensors to smart implants - toward pervasive and personalized healthcare. *IEEE Trans. Biomed. Eng.* 62 (12), 2750–2762. <https://doi.org/10.1109/TBME.2015.2422751>.
- Bell, A.J., Sejnowski, T.J., 1995. An information-maximization approach to blind separation and blind deconvolution. *Neural Comput.* 7 (6), 1129–1159.
- Bertsekas, D.P., 1988. The auction algorithm: a distributed relaxation method for the assignment problem. *Ann. Oper. Res.* 14 (1), 105–123.
- Bießmann, F., Meinecke, F.C., Gretton, A., Rauch, A., Rainer, G., Logothetis, N., Müller, K.-R., 2009. Temporal kernel canonical correlation analysis and its application in multimodal neuronal data analysis. *Mach. Learn.* 79 (1–2), 5–27. <https://doi.org/10.1007/s10994-009-5153-3>.
- Boas, D., Brooks, D., Miller, E., DiMarzio, C., Kilmer, M., Gaudette, R., Zhang, Q., 2001. Imaging the body with diffuse optical tomography. *Signal Processing Magazine. IEEE* 18 (6), 57–75. <https://doi.org/10.1109/79.962278>.
- Boukouvelas, Z., Levin-Schwartz, Y., Calhoun, V.D., Adali, T., 2018. Sparsity and independence: balancing two objectives in optimization for source separation with application to fmri analysis. *J. Frankl. Inst.* 355 (4), 1873–1887.
- Boukouvelas, Z., Levin-Schwartz, Y., Mowakeaa, R., Fu, G.-S., Adali, T., 2018. Independent component analysis using semi-parametric density estimation via

- entropy maximization. In: IEEE Statistical Signal Processing Workshop (SSP), vol. 2018. IEEE, pp. 403–407.
- Boushel, R., Langberg, H., Olesen, J., Gonzales-Alonzo, J., Bülow, J., Kjaer, M., 2001. Monitoring tissue oxygen availability with near infrared spectroscopy (nirs) in health and disease. *Scand. J. Med. Sci. Sports* 11 (4), 213–222.
- Brigadoi, S., Ceccherini, L., Cutini, S., Scarpa, F., Scatturin, P., Selb, J., Gagnon, L., Boas, D.A., Cooper, R.J., 2014. Motion artifacts in functional near-infrared spectroscopy: a comparison of motion correction techniques applied to real cognitive data. *Neuroimage* 85, 181–191.
- Caicedo, A., Papademetriou, M.D., Ellwell, C.E., Hoskote, A., Elliott, M.J., Van Huffel, S., Tachtsidis, I., 2013. Canonical correlation analysis in the study of cerebral and peripheral haemodynamics interrelations with systemic variables in neonates supported on ecmo. *Oxygen Transport to Tissue XXXIV*. Springer, pp. 23–29.
- Calhoun, V.D., Adali, T., McGinty, V., Pekar, J.J., Watson, T., Pearlson, G., 2001. Fmri activation in a visual-perception task: network of areas detected using the general linear model and independent components analysis. *Neuroimage* 14 (5), 1080–1088.
- Choi, S., Cichocki, A., Zhang, L., Amari, S.-I., 2003. Approximate maximum likelihood source separation using the natural gradient. *IEICE Trans. Fundam. Electron. Commun. Comput. Sci.* 86 (1), 198–205.
- Comon, P., Jutten, C., 2010. *Handbook of Blind Source Separation: Independent Component Analysis and Applications*. Academic press.
- Cui, X., Bray, S., Reiss, A.L., 2010. Functional near infrared spectroscopy (nirs) signal improvement based on negative correlation between oxygenated and deoxygenated hemoglobin dynamics. *Neuroimage* 49 (4), 3039–3046.
- Dähne, S., Bießman, F., Meinecke, F.C., Mehnert, J., Fazli, S., Müller, K.-R., 2013. Integration of multivariate data streams with bandpower signals. *IEEE Trans. Multimed.* 15 (5), 1001–1013. <https://doi.org/10.1109/TMM.2013.2250267>.
- Dähne, S., Bießman, F., Samek, W., Haufe, S., Goltz, D., Gundlach, C., Villringer, A., Fazli, S., Müller, K.-R., 2015. Multivariate machine learning methods for fusing functional multimodal neuroimaging data. *Proc. IEEE* 103 (9), 1507–1530. <https://doi.org/10.1109/JPROC.2015.2425807>.
- Delpy, D.T., Cope, M., van der Zee, P., Arridge, S., Wray, S., Wyatt, J., 1988. Estimation of optical pathlength through tissue from direct time of flight measurement. *Phys. Med. Biol.* 33 (12), 1433.
- Eriksson, J., Koivunen, V., 2004. Complex-valued ica using second order statistics. In: *Machine Learning for Signal Processing, 2004. Proceedings of the 2004 14th IEEE Signal Processing Society Workshop*, pp. 183–192. IEEE.
- Fazli, S., Mehnert, J., Steinbrink, J., Curio, G., Villringer, A., Müller, K.-R., Blankertz, B., 2012. Enhanced performance by a hybrid NIRS-EEG brain computer interface. *Neuroimage* 59 (1), 519–529. <https://doi.org/10.1016/j.neuroimage.2011.07.084>.
- Fazli, S., Dähne, S., Samek, W., Bießmann, F., Müller, K.-R., 2015. Learning from more than one data source: data fusion techniques for sensorimotor rhythm-based Brain-Computer Interfaces. *Proc. IEEE* 103 (6), 891–906. <https://doi.org/10.1109/JPROC.2015.2413993>.
- Ferrari, M., Mottola, L., Quaresima, V., 2004. Principles, techniques, and limitations of near infrared spectroscopy. *Can. J. Appl. Physiol.* 29 (4), 463–487.
- Franceschini, M.A., Joseph, D.K., Huppert, T.J., Diamond, S.G., Boas, D.A., 2006. Diffuse optical imaging of the whole head. *J. Biomed. Opt.* 11 <https://doi.org/10.1117/1.2363365>, 11 – 11 – 10.
- Fu, G.-S., Phlypo, R., Anderson, M., Li, X.-L., et al., 2014. Blind source separation by entropy rate minimization. *IEEE Trans. Signal Process.* 62 (16), 4245–4255.
- Fu, G.-S., Anderson, M., Adali, T., 2014. Likelihood estimators for dependent samples and their application to order detection. *IEEE Trans. Signal Process.* 62 (16), 4237–4244.
- Hamaoka, T., McCully, K.K., Quaresima, V., Yamamoto, K., Chance, B., 2007. Near-infrared spectroscopy/imaging for monitoring muscle oxygenation and oxidative metabolism in healthy and diseased humans. *J. Biomed. Opt.* 12 (6), 062105–062105.
- Haufe, S., Meinecke, F., Görgen, K., Dähne, S., Haynes, J.-D., Blankertz, B., Bießmann, F., 2014. On the interpretation of weight vectors of linear models in multivariate neuroimaging. *Neuroimage* 87, 96–110. <https://doi.org/10.1016/j.neuroimage.2013.10.067>.
- Hoshi, Y., 2007. Functional near-infrared spectroscopy: current status and future prospects. *J. Biomed. Opt.* 12 (6), 062106–062106.
- Hotelling, H., 1936. Relations between two sets of variates. *Biometrika* 28 (3/4), 321–377.
- Huppert, T.J., 2016. Commentary on the statistical properties of noise and its implication on general linear models in functional near-infrared spectroscopy. *Neurophotonics* 3 (1), 010401.
- Huppert, T.J., Diamond, S.G., Franceschini, M.A., Boas, D.A., 2009. HomER: a review of time-series analysis methods for near-infrared spectroscopy of the brain. *Appl. Opt.* 48 (10), D280–D298. <https://doi.org/10.1364/AO.48.00D280>.
- Hyvärinen, A., 1999. Fast and robust fixed-point algorithms for independent component analysis. *IEEE Trans. Neural Netw.* 10 (3), 626–634.
- Hyvärinen, A., Karhunen, J., Oja, E., 2004. *Independent Component Analysis*, vol. 46. John Wiley & Sons.
- Irani, F., Platek, S.M., Bunce, S., Ruocco, A.C., Chute, D., 2007. Functional near infrared spectroscopy (fnirs): an emerging neuroimaging technology with important applications for the study of brain disorders. *Clin. Neuropsychol.* 21 (1), 9–37.
- Izzetoglu, M., Chitrapu, P., Bunce, S., Onaral, B., 2010. Motion artifact cancellation in nir spectroscopy using discrete kalman filtering. *Biomed. Eng. Online* 9 (1), 16.
- Josephs, O., Turner, R., Friston, K., 1997. Event-related fmri. *Hum. Brain Mapp.* 5 (4), 243–248.
- Kohno, S., Miyai, I., Seiyama, A., Oda, I., Ishikawa, A., Tsuneishi, S., Amita, T., Shimizu, K., 2007. Removal of the skin blood flow artifact in functional near-infrared spectroscopic imaging data through independent component analysis. *J. Biomed. Opt.* 12 (6), 062111.
- Li, X.-L., Adali, T., 2010. Independent component analysis by entropy bound minimization. *IEEE Trans. Signal Process.* 58 (10), 5151–5164.
- Li, Y.-O., Adali, T., Calhoun, V.D., 2007. Estimating the number of independent components for functional magnetic resonance imaging data. *Hum. Brain Mapp.* 28 (11), 1251–1266.
- Long, Q., Jia, C., Boukouvalas, Z., Gabrielson, B., Emge, D., Adali, T., 2018. Consistent run selection for independent component analysis: application to fmri analysis. In: *2018 IEEE International Conference on Acoustics, Speech and Signal Processing (ICASSP)*. IEEE, pp. 2581–2585.
- Macchi, O., 1993. Self-adaptive source separation by direct and recursive networks. *Proc. International Conference on Digital Signal Processing (DSP'93)* Limasol, pp. 1154–1159. Cyprus.
- Markham, J., White, B.R., Zeff, B.W., Culver, J.P., 2009. Blind identification of evoked human brain activity with independent component analysis of optical data. *Hum. Brain Mapp.* 30 (8), 2382–2392.
- Medvedev, A.V., Kainerstorfer, J., Borisov, S.V., Barbour, R.L., VanMeter, J., 2008. Event-related fast optical signal in a rapid object recognition task: improving detection by the independent component analysis. *Brain Res.* 1236 (0), 145–158. <https://doi.org/10.1016/j.brainres.2008.07.122>.
- Metz, A., Wolf, M., Achermann, P., Scholkmann, F., 2015. A new approach for automatic removal of movement artifacts in near-infrared spectroscopy time series by means of acceleration data. *Algorithms* 8 (4), 1052–1075.
- Molavi, B., Dumont, G.A., 2012. Wavelet-based motion artifact removal for functional near-infrared spectroscopy. *Physiol. Meas.* 33 (2), 259.
- Morren, G., Wolf, M., Lemmerling, P., Wolf, U., Choi, J., Gratton, E., De Lathauwer, L., Van Huffel, S., 2004. Detection of fast neuronal signals in the motor cortex from functional near infrared spectroscopy measurements using independent component analysis. *Med. Biol. Eng. Comput.* 42 (1), 92–99. <https://doi.org/10.1007/BF02351016>.
- Muehleemann, T., Haense, D., Wolf, M., 2008. Wireless miniaturized in-vivo near infrared imaging. *Optic Express* 16 (14), 10323–10330.
- Müller-Putz, G., Leeb, R., Tangermann, M., Höhne, J., Kübler, A., Cincotti, F., Mattia, D., Rupp, R., Müller, K.-R., Millan, J., 2015. Towards noninvasive hybrid brain computer interfaces: framework, practice, clinical application, and beyond. *Proc. IEEE* (99), 1–18.
- Parasuraman, R., 2003. Neuroergonomics: research and practice. *Theor. Issues Ergon. Sci.* 4 (1–2), 5–20.
- Parra, L.C., Spence, C.D., Gerson, A.D., Sajda, P., 2005. Recipes for the linear analysis of {EEG}. *Neuroimage* 28 (2), 326–341. <https://doi.org/10.1016/j.neuroimage.2005.05.032>.
- G. Pfurtscheller, B. Z. Allison, G. Bauernfeind, C. Brunner, T. Solis Escalante, R. Scherer, T. O. Zander, G. Müller-Putz, C. Neuper, N. Birbaumer, The hybrid BCI, *Front. Neurosci.* 4 (3). doi:10.3389/fnpro.2010.00003.
- Rodriguez, P.A., Anderson, M., Li, X.-L., Adali, T., 2014. General non-orthogonal constrained ica. *IEEE Trans. Signal Process.* 62 (11), 2778–2786.
- Saager, R.B., Berger, A.J., 2005. Direct characterization and removal of interfering absorption trends in two-layer turbid media. *J. Opt. Soc. Am.* 22 (9), 1874–1882.
- Safaie, J., Grebe, R., Moghaddam, H.A., Wallois, F., 2013. Toward a fully integrated wireless wearable EEG-nirs bimodal acquisition system. *J. Neural Eng.* 10 (5), 056001.
- Samek, W., Nakajima, S., Kawabata, M., Müller, K.-R., 2017. On robust parameter estimation in brain-computer interfacing. *J. Neural Eng.* 14 (6), 061001.
- Schelkanova, I., Toronov, V., 2012. Independent component analysis of broadband near-infrared spectroscopy data acquired on adult human head. *Biomed. Opt. Express* 3 (1), 64–74.
- Scholkmann, F., Spichtig, S., Muehleemann, T., Wolf, M., 2010. How to detect and reduce movement artifacts in near-infrared imaging using moving standard deviation and spline interpolation. *Physiol. Meas.* 31 (5), 649.
- Scholkmann, F., Kleiser, S., Metz, A.J., Zimmermann, R., Pavia, J.M., Wolf, U., Wolf, M., 2014. A review on continuous wave functional near-infrared spectroscopy and imaging instrumentation and methodology. *Neuroimage* 85, 6–27.
- Scholkmann, F., Metz, A.J., Wolf, M., 2014. Measuring tissue hemodynamics and oxygenation by continuous-wave functional near-infrared spectroscopy: how robust are the different calculation methods against movement artifacts? *Physiol. Meas.* 35 (4), 717.
- Shin, J., von Lüthmann, A., Blankertz, B., Kim, D.-W., Jeong, J., Hwang, H.-J., Müller, K.-R., 2017. Open access dataset for eeg+ nirs single-trial classification. *IEEE Trans. Neural Syst. Rehabil. Eng.* 25 (10), 1735–1745.
- Shin, J., von Lüthmann, A., Kim, D.-W., Mehnert, J., Hwang, H.-J., Müller, K.-R., 2018. Simultaneous acquisition of eeg and nirs during cognitive tasks for an open access dataset. *Nat. Sci. Data* 5, 180003. <https://doi.org/10.1038/sdata.2018.3>.
- Tachtsidis, I., Scholkmann, F., 2016. False positives and false negatives in functional near-infrared spectroscopy: issues, challenges, and the way forward. *Neurophotonics* 3 (3), 031405.
- Virtanen, J., Noponen, T.E., Meriläinen, P., 2009. Comparison of principal and independent component analysis in removing extracerebral interference from near-infrared spectroscopy signals. *J. Biomed. Opt.* 14 (5), 054032.
- Virtanen, J., Noponen, T., Kotilahti, K., Virtanen, J., Ilmoniemi, R.J., 2011. Accelerometer-based method for correcting signal baseline changes caused by motion artifacts in medical near-infrared spectroscopy. *J. Biomed. Opt.* 16 (8), 087005–087005.
- von Büna, P., Meinecke, F.C., Király, F., Müller, K.-R., 2009. Finding stationary subspaces in multivariate time series. *Phys. Rev. Lett.* 103, 214101.
- von Lüthmann, A., Herff, C., Heger, D., Schultz, T., 2015. Towards a wireless open source instrument: functional near-infrared spectroscopy in mobile neuroergonomics and bci

- applications. *Front. Hum. Neurosci.* 9 (617) <https://doi.org/10.3389/fnhum.2015.00617>.
- von Lüthmann, A., Wabnitz, H., Sander, T., Müller, K.-R., 2017. M3BA: a mobile, modular, multimodal biosignal acquisition architecture for miniaturized EEG-NIRS-based hybrid bci and monitoring. *IEEE (Inst. Electr. Electron. Eng.) Trans. Biomed. Eng.* 64 (6), 1199–1210. <https://doi.org/10.1109/TBME.2016.2594127>.
- Wolf, M., Ferrari, M., Quaresima, V., 2007. Progress of near-infrared spectroscopy and topography for brain and muscle clinical applications. *J. Biomed. Opt.* 12 (6), 062104–062104.
- Wyser, D.G., Lambercy, O., Scholkman, F., Wolf, M., Gassert, R., 2017. Wearable and modular functional near-infrared spectroscopy instrument with multidistance measurements at four wavelengths. *Neurophotonics* 4 (4), 041413.
- Ye, J.C., Tak, S., Jang, K.E., Jung, J., Jang, J., 2009. Nirs-spm: statistical parametric mapping for near-infrared spectroscopy. *Neuroimage* 44 (2), 428–447.
- Zhang, Y., Franceschini, M.A., Boas, D.A., Brooks, D.H., 2005. Eigenvector-based spatial filtering for reduction of physiological interference in diffuse optical imaging. *J. Biomed. Opt.* 10 (1) <https://doi.org/10.1117/1.1852552>, 011014–011014–11.
- Zhang, Q., Strangman, G.E., Ganis, G., 2009. Adaptive filtering to reduce global interference in non-invasive nirs measures of brain activation: how well and when does it work? *Neuroimage* 45 (3), 788–794.
- Zheng, Y.-L., Ding, X.-R., Poon, C., Lo, B., Zhang, H., Zhou, X.-L., Yang, G.-Z., Zhao, N., Zhang, Y.-T., 2014. Unobtrusive sensing and wearable devices for health informatics. *IEEE Trans. Biomed. Eng.* 61 (5), 1538–1554. <https://doi.org/10.1109/TBME.2014.2309951>.
- Ziehe, A., Müller, K.-R., 1998. TDSEP – an efficient algorithm for blind separation using time structure. In: Niklasson, L., Bodén, M., Ziemke, T. (Eds.), *Proc. Of the 8th International Conference on Artificial Neural Networks, ICANN'98, Perspectives in Neural Computing*. Springer Verlag, Berlin, pp. 675–680.